Tensile and cracking behaviour of crimped textile reinforced mortar (TRM) based on digital image correlation

Khan Junaid, Zyed Mesticou, Algourdin Nonna, Gaochuang Cai, Amir Si Larbi

Construction and Building Materials 417 (2024) 135321

Contents lists available at ScienceDirect

Construction and Building Materials

journal homepage: www.elsevier.com/locate/conbuildmat

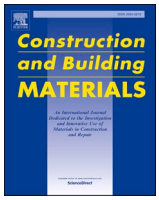

Tensile and cracking behaviour of crimped textile reinforced mortar (TRM) based on digital image correlation

Khan Junaid [a,*], Mesticou Zyed [a], Algourdin Nonna [a], Cai Gaochuang [a,b], Si Larbi Amir [a]

[a] Université de Lyon, Ecole Centrale de Lyon – ENISE, Laboratoire de Tribologie et Dynamique des Systèmes (LTDS) CNRS UMR 5513, 58 rue Jean Parot, 42100 Saint-Etienne, France
[b] International Advanced Science and Technology Research Organization (IROAST), Kumamoto University, Kurokami, 8608555 Kumamoto, Japan

ARTICLE INFO

Keywords:
Tensile behaviour
TRM
Crack opening
Crimped textile
Image correlation
ACK

ABSTRACT

The tensile behaviour of textile reinforced mortar (TRM) is sensitive to the adopted matrix, textile, and their interfacial bonding. The matrix–textile bond varies with the nature of the adopted textile. In this study, the influence of textile crimp and orientation on the tensile and cracking responses of cement matrix-based TRM was studied for coated and noncoated (uncoated) carbon textiles using digital image correlation. This study also examined the behaviour of a hybrid TRM incorporating layers of coated and noncoated carbon. The results showed that the presence of load-aligned crimped yarns influenced the deformation, damage mode, cracking evolution, and crack opening of the TRMs. Finally, based on the observed deformations of the load-oriented crimped-yarn TRMs, a simple modification term for the second phase strains of the ACK model was proposed based on the textile geometry. The modified term produced strain values within 9.7–15% of the experimental strain.

1. Introduction

Textile reinforced mortar (TRM) is a composite composed of a mineral-based matrix reinforced with a continuous fabric [1]. The fabrics are generally composed of carbon, glass, aramid, polyphenylene benzobisoxazole, and steel. Research on TRMs has gained momentum over the last few decades and has continued because of their suitable performance as strengthening alternatives to fibre-reinforced polymers (FRPs). For instance, the compatibility with concrete substrates, breathability, applicability to wet surfaces, and enhanced fire resistance provide the basis for advancing our understanding of TRMs [2,3]. Additionally, the replacement of traditional steel rebars with noncorrosive reinforcements makes them preferred candidates for new structures [4].

The performance of TRMs under tensile testing has been studied by various authors to understand their constitutive behaviour [5–10]. The typical uniaxial tensile response of the TRM (Fig. 1) is composed of three phases: 1) the first phase corresponds to pre-cracking, where the response is dominated by the matrix properties; 2) the second phase is a multi-cracking phase governed by the redistribution of stress between the textile and matrix; and 3) the third phase is characterised by load transfer across the cracked matrix through the textile, along with the widening of the cracks [1,11].

The pre-mentioned trilinear behaviour and mechanical capacity of TRMs are sensitive to the properties of textiles, mortars, and their bonds [11]. The mechanical performance is affected by parameters such as the textile mesh, textile orientation, textile geometry, reinforcement ratio (V_f), and nature of the coating. Similarly, matrix characteristics such as strength, flowability, [12] and aggregate particle size [13] also influence the constitutive behaviour of TRMs.

The reinforcement ratio is an influencing factor, and various authors have analysed its impact on the response of TRMs [7,14–20]. For instance, Saidi and Gabor [7] observed that the load-transfer length between the textile and mortar decreases with an increase in V_f, demonstrating enhanced textile–mortar bonding. The results in [7] showed that an increase in the number of layers results in a higher ultimate strength. Additionally, the influence of textile reinforcement on the tensile response was sensitive to the nature of the mortar. In contrast, [15] showed that, on average, a higher number of overlapping basalt layers results in a reduced ultimate strength (calculated for the textile area) owing to the modification of the failure mode, which restricted complete textile breakage. Similar results have been reported [21] for one-, two, and three layers of Basalt TRM. Similarly, [22] reported the modification of the failure mode with an increasing number of carbon

* Corresponding author.
E-mail address: junaid.khan@enise.fr (K. Junaid).

https://doi.org/10.1016/j.conbuildmat.2024.135321
Received 22 November 2023; Received in revised form 17 January 2024; Accepted 2 February 2024
Available online 10 February 2024

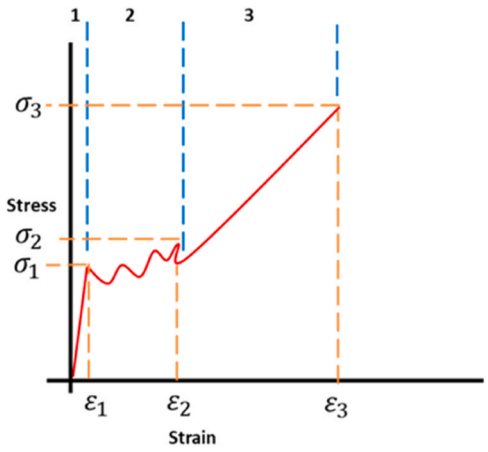

Fig. 1. Typical tri-phasic response of TRMs in tensile test.

layers, but without reduced ultimate strength.

Another factor that influences the properties of TRMs is the use of hybrid reinforcement. For example, [23] and [5] studied the effects of hybrid reinforcements on the tensile responses of TRMs. The study in [23] used TRMs formed with laminae of polypropylene (PP) and AR glass. The study showed that the arrangement of the layers had a significant influence on the load-bearing behaviour, with enhanced performance when the AR glass layer was sandwiched between two layers of PP. The combination of glass and PP resulted in a composite stronger than the PP-only layer TRM and was more ductile than the AR glass TRM. In [23], significantly different lamina properties resulted in delamination, which was more prominent when the ductile PP layer was located between two AR glass layers.

In addition to the influence of V_f and the hybrid reinforcement, the performance of TRMs is affected by the presence of telescopic failure, where the core filaments are not fully utilised in the load-bearing function [15,23,24]. Polymer-coated fabrics in TRMs have been explored to improve the interaction across filaments [17,24–26]. In the study of [25] epoxy combined with rice husk ash was used to improve the performance of basalt- and glass-based TRMs. The coating improved textile utilisation with denser cracking and three times enhancement of basalt TRM strength. [17] showed that coating basalt textiles with epoxy led to a 25% improvement in the ultimate strength. However, the incompatibility of polymer coatings with cementitious products poses the challenges of delamination, inconsistent cracking, larger crack widths, and deterioration under high temperatures [18,27]. Therefore, efforts have been made to use mineral-based products for yarn impregnation [28,29].

Similarly, the TRM behaviour is sensitive to textile orientation. To date, few studies have been conducted on the impact of textile orientation on the load-bearing capacity of TRMs [23,30–32]. [30] observed that TRMs with weft yarns placed in the load direction had a higher capacity than those with warp yarns placed in the load direction. Although the tensile strength of the fabric was superior in the warp direction owing to the round and compact nature of the roving, which enhanced the frictional interaction between the filaments, but within TRM the flat and loose nature of the weft yarns resulted in a larger contact surface between the mortar and textile. The mortar–textile bond was further bolstered by the better penetration of the matrix, leading to a superior load-bearing capacity [27]. [23] observed that the influence of textile orientation on the load-bearing capacity was reversed when TRM was formed through the pultrusion process, with warp roving pulled in the pultrusion direction. This is because of the enhanced penetration of the matrix into the warp yarns. In addition to textile orientation, studies have shown that the behaviour of TRMs is sensitive to the shape of the yarns [32], [33]. For instance, [33] reported that crimped yarn-based TRMs demonstrated superior flexural performance to TRMs with straight yarns.

In addition to its aforementioned impact on mechanical capacity, the cracking behaviour of TRMs is also affected by the properties of the textile [15,32]. [34] showed that the application of a sand coating on textiles reduced the crack width by approximately 33%. While in some mortar–textile combinations, the longitudinal splitting of the TRMs at the mortar–textile interface affected the overall cracking behaviour.

The tensile behaviour of TRMs has been extensively explored, and the influencing parameters have been identified. However, according to [34], the absence of standardisation of textile reinforcement and the availability of various reinforcement options necessitates expanding the understanding of the behaviour (including cracking) of TRMs. For instance, one such factor of importance is textile crimp. Limited studies have been reported on the influence of crimp on tensile and cracking behaviours. Therefore, this study contributes to the understanding of carbon-based TRMs by systematically analysing the influence of crimp on the load-bearing and cracking response under tension. Based on the influencing parameters identified in the literature, the analysis of the effect of the crimp was extended to 1) the number of layers, 2) influence of the polymer coating, 3) textile orientation, and 4) hybrid TRMs. The case of hybrid TRMs extends their existing limited database while reducing the risks of delamination owing to the mismatch of the textile properties. The studied cases were further analysed in terms of their cracking behaviour using stereo digital image correlation [25,35]. Finally, a modification term was added to the ACK model to account for the large strains in the crimped textile composites.

2. Material and methods

2.1. Textile and mortar

2.1.1. Textile

In this study, two types of balanced biaxial carbon fabrics were used in the TRMs. $T_{uncoated}$ and TCSBR, with a tex of 12000 and a mesh size of 5 mm × 5 mm. The filament diameter was 7 μm (Table 1). The warp yarns of $T_{uncoated}$ were crimped in-plane (Fig. 2). TCSBR was obtained through the industrial application of a styrene butadiene coating (SBR) on the $T_{uncoated}$ fabric. Because of the coating process, the weft yarns of the TCSBR developed a substantial out-of-plane crimp, whereas the warp crimp was significantly reduced. A third modification of the $T_{uncoated}$ textile was obtained by manual/hand application of a microsilica (Emsac 500 SE) coating. The microsilica was in a suspension form, with the largest particle diameter of 0.15 μm.

2.1.2. Mortar

A commercial hydraulic mortar formulated for strengthening and repair applications was used. The maximum particle size of the fine aggregates was limited to 1 mm, which was crucial for the penetration of the mortar into the textile mesh.

The compressive and flexural strengths of the mortar (shown in Table 2) were obtained using three specimens with dimensions of 40 mm × 40 mm × 160 mm tested according to the EU Norm EN-196–1 [36]. The adherence/bond strength was provided by the manufacturer.

2.2. Preparation of TRM specimens and testing method

A total of 24 TRM samples were tested, three for each of the eight cases studied (Table 3). With the weft yarns placed parallel to the load direction, TunW, T1W, and T2W were formed with one-layer of uncoated textile and one and two layers of coated textile, respectively (Fig. 3). TunM, T1M, and T2M had textile configurations similar to those of TunW, T1W, and T2W, respectively, but different yarn orientations, with the warp yarns aligned in the load direction (Fig. 3). TsiW was formed by placing a single layer of the microsilica-coated textile with weft yarns parallel to the load axis. The textile was dipped and hand-pressed in a microsilica slurry and set to dry for at least 24 h before its

Table 1
Properties of textile.

Textile	Mesh (mm)	Material	Coating	area weight g/cm^2	No. filaments	Fil dia	Warp		Weft	
							σ_f (MPa)	E_f (GPa)	σ_f (MPa)	E_f (GPa)
TCSBR	5 × 5	Carbon	Styrene butadiene	0.034	12000	7 μm	1400	120	1400	120
$T_{uncoated}$	5 × 5	Carbon	non	0.025	12000	7 μm	1400	114	1850	114

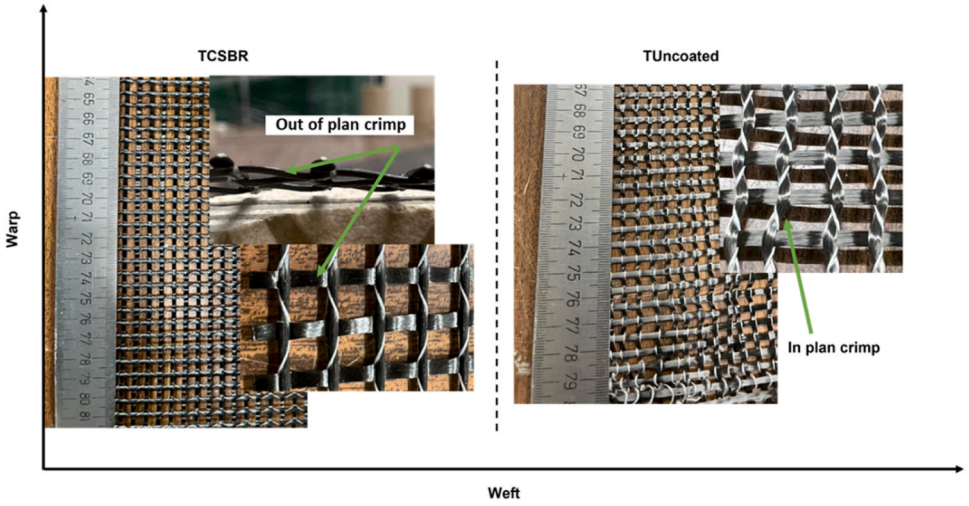

Fig. 2. Representation of the styrene butadiene coated (TCSBR) and uncoated ($T_{uncoated}$) textile.

Table 2
Properties of mortar.

Mortar	
$\sigma_{m.f}$ [MPa] (CoV)	9 (0.14)
$\sigma_{m.c}$ [MPa] (CoV)	51 (0.10)
max grain size [mm]	1
Adherence [MPa]	2

placement in the mortar. Finally, ThM was formed by placing a layer of polymer-coated textile between two uncoated textile layers (separated by 2–3 mm of mortar in between), all in a warp orientation (Fig. 3).

For each TRM, a 500 mm × 700 mm × (n + 1) × t mm plate was prepared using the wet-hand layup method [37], where 'n' represents the number of textile layers and 't' is the thickness of a single mortar layer, which ranged between 2–3 mm. The plates were laminated in plywood moulds and nailed with wooden strips. The wooden strips were dimensioned according to the expected TRM thickness.

The plates were wet-cured for 7 days, followed by storage at a relative humidity of approximately 50% for 21 days. After 28 days, a wet saw was used to cut three samples, each 650 mm × 70 mm in size. Note that all edges of the plates were discarded with a width of 20 mm to eliminate any weaknesses generated by mould-plate interaction during the manual lamination process. The specimens were stored for 60 more days (90 days in total) at 25 ℃ and relative humidity of about 50% before finally tested.

Finally, it is important to mention that the minimum thickness of 6 mm recommended by RILEM TC-232-TDT could not always be strictly respected because of the hand-lay-up implementation (coupled with shrinkage). However, the difference (from the RILEM's threshold of 6 mm) remained limited and did not significantly compromise the relevance of the test or its application.

2.3. Tensile test setup

The recommendations of RILEM TC-232-TDT [38] were adopted to perform the tensile tests on the composites. The clamps used for gripping the TRMs were 100 mm × 200 mm and attached to the machine through a ball/spherical joint to mitigate the transfer of parasitic moments.

At 200 mm, the ends of the specimens were attached to rubber pads on both faces to mitigate the risk of bearing failure in the clamps (Fig. 3). The TRM was carefully centred in the width of the clamp to avoid undesired in-plane bending. The test was performed on a 100 kN WOLPERT machine with a displacement rate of 0.5 mm/min. The adopted test setup is shown in Fig. 4.

For deformation acquisition, the finished surface of the composite was always reserved for the digital image correlation (DIC) measurements. The second face (the one that was always in contact with the

Table 3
Description of the studied TRM configurations.

TRM Type	Thickness (mm) /CoV (%)	Width (mm) / CoV (%)	Total Length (mm)	V_f (%)	Textile orientation	Textile Layers
T1W	5.5/3.27	69.01/ 0.31	650	1.2	Weft	1 TCSBR
T2W	7.76/4.38	68.99/ 0.49	650	1.6	Weft	2 TCSBR
TunW	6.91/1.3	68.94/ 0.44	650	1.2	Weft	1 $T_{uncoated}$
TsiW	5.49/2.72	69.87/ 0.38	650	1.2	Weft	1 $T_{uncoated}$-silica modified
T1M	5.71/0.78	70.23/ 0.28	650	1.2	Warp	1 TCSBR
T2M	9.66/5.4	70.29/ 0.22	650	1.6	Warp	2 TCSBR
TunM	5.93/3.7	69.84/ 0.57	650	1.2	Warp	1 $T_{uncoated}$
ThM	13.13/1.06	69.86/ 0.45	650	1.8	Warp	1 $T_{uncoated}$-1 TCSBR-1 $T_{uncoated}$

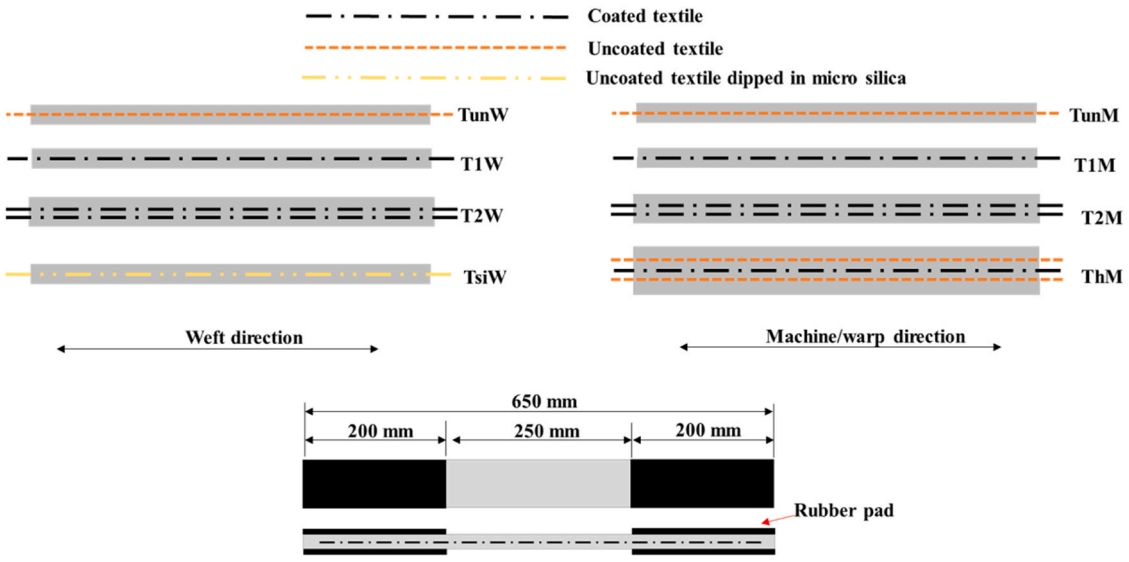

Fig. 3. Representation of the studied TRM samples.

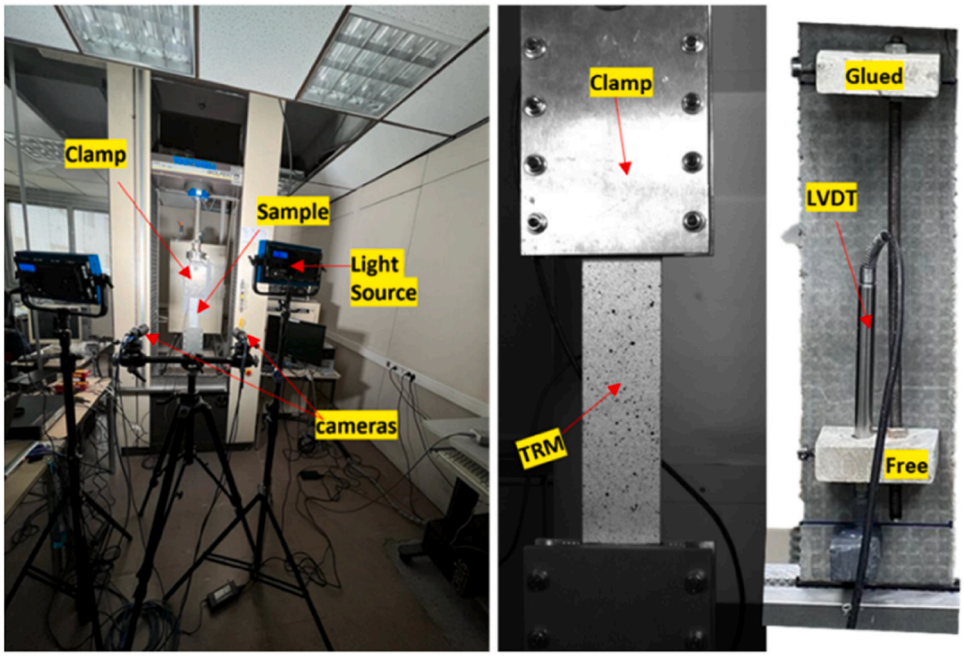

Fig. 4. Adopted tensile test setup; left to right: global view and zoomed sample.

mould) was equipped with a linear variable differential transformer (LVDT). The LVDT was supported on the TRM surface using a glued pedestal. The measurement of the displacement on opposite faces enabled the computation of average strains to accommodate for deformation induced by out-of-plane bending, possibly caused by misalignment and/or curvature in the TRMs owing to shrinkage [16]. Stereo DIC was performed using two cameras of 5 mega pixels. For measurement consistency, the DIC process was assisted by a light source of constant luminosity adjusted for the region of interest, which was defined by the gauge length of the samples, covering the width and length of the composite between the clamps. The images were acquired at a frequency of 2 Hz.

The software MatchID was used for image correlation. A subset size of 45 and step size of 15 pixels were adopted as a suitable trade-off between the computational time and accuracy of the obtained deformation. Quadratic shape functions were used for the subsets and cross-camera matching. The correlated data were processed in MATLAB to obtain the desired representation of the outputs. One of the objectives of the DIC measurements was to gain further insight into the cracking behaviour of the TRMs by acquiring full-field deformation during the test.

The mobilised tensile test is considered to be controversial to the extent that the results obtained are not entirely decoupled from the tightening carried out at the clamps and that the load transfer mechanisms favour the mobilisation of the textile more than that of the composite (strictly speaking). However, the test in question is not devoid of interest and is of certain utility for understanding, although imperfectly, the tensile strength of TRM composites. Moreover, it enables a comparison of various TRM configurations to identify the determining or decisive parameters. Based on this observation, an experimental campaign and its exploitation were conducted.

2.4. Tomography

For microscale observation, 20 mm × 20 mm pieces were cut from the T1W, TunW, and TsiW TRM plates. The plates used to obtain these samples were undamaged and were not used for the tensile tests. The obtained samples were exposed to tomography, with achievable voxel size of 6 μm. The test arrangement comprising the X-ray tube, exposed TRM piece, and background screen is shown in Fig. 5. The acquired images were analysed using the software Fiji.

3. Results and discussion

3.1. Failure modes

The observed failure modes for the tested TRMs were classified as shown in Fig. 6. Representative failures for each tested TRM type are shown in Fig. 7. TunW and TsiW exhibited failure by telescopic slip of the textile either in the gauge length or at the clamp mouth (Mode C). The damage remained identical on both the faces of TunW and TsiW.

T1W failed through textile rupture (either in the gauge length or near the clamp) with the associated severe chipping of the mortar on one face of the TRM (Modes A, B, and E). In T2W, in addition to the chipping damage, textile rupture was accompanied by severe interlaminar delamination (Modes A, B, E, and F). The observed conditions for the chipping damage at failure are shown in Fig. 7b (T1W); such chipping damage attributed to the textile crimp was reported in [24,39]. Delamination in T2W was initiated locally near the end of the hardening (second) phase (Fig. 1). However, complete separation between the two layers was only observed after the rupture of the textile.

The warp-oriented TRMs failed by the partial or complete breakage of the textile. The failure of TunM was marked by limited telescopic slip, followed by the brittle partial rupture of yarns (Mode D). T1M (Mode 'A and B') and T2M (Mode 'B') failed due to the rupturing of the textile without interlaminar delamination. Finally, ThM exhibited partial/full textile rupture with limited slip (near the clamps) accompanied by local delamination (Modes A, D, and G). The delamination in ThM was localised at the TCSBR textile–mortar interface. The extent of the delamination was limited. compared with the severe delamination scenarios observed in other hybrid TRM studies [23].

The absence of crimped yarns in the load directions of T1M and T2M mitigated severe spalling and delamination, respectively. Additionally, the presence of uncoated crimped yarns in the load orientation did not influence the global failure mode. This showed that the effect of the crimp on the failure mode is sensitive to the textile coating and the nature of the crimp.

3.2. Tomographic analysis

Images of the TRMs cross-sections for T1W, TunM, and TsiW are shown in Fig. 8. In comparison with T1W and TunM, agglomeration of micro-silica at the textile matrix interface in TsiW was observed. This resulted in an additional layer between the textile and mortar. The microsilica deposition was cracked, as shown in Fig. 8c (TsiW), which resulted in degradation of the textile–mortar interfacial bond. Hence, the diminished load-bearing performance of the TsiW was triggered by the adverse impact of the manual modification of the textile with microsilica.

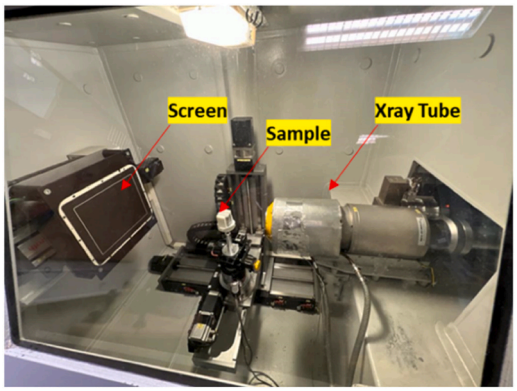

Fig. 5. Overview of the tomography setup.

3.3. Global tensile response: stress–strain behaviour

The stress–strain responses of the three samples of each of the eight different composites are shown in Fig. 9. The stress (left ordinate in Fig. 9) was calculated over the average cross-section of the composite. The average cross-section was computed based on the average value of the composite thickness over the gauge length. The composite stress was used to relate various parameters throughout the text. However, for comparison, the stress calculated for the textile area is also given in Fig. 9 (as shown by the right ordinate). Globally, the obtained stress–-strain responses demonstrated good repeatability for the three tested samples of each TRM type.

The TRMs exhibited distinct triphasic behaviours, except for TsiW-A and TsiW-B, where the distinction between the second and third phase was not apparent. The biphasic response was triggered by the compromised textile–mortar interface of TsiW. The post-peak response could not be recorded because of brittle failure, except for TunW and TsiW, where a softening branch was observed because of the telescopic mode. For TsiW and TunW, the post-peak response exhibited either an increase or a counterintuitive decrease in strain. The reduction in strain was due to the slip near the clamps, which could not be captured by the LVDT/DIC.

Qualitatively, as shown in Fig. 9, the shape of the stress–strain curve was sensitive to the textile coating, textile orientation, number of layers, and hybrid reinforcement. These factors influenced the strain-hardening behaviour, stiffness, failure mode, and ultimate properties [11]. The effects of the crimps on the global responses of TunM, T1W, and T2W were also evident (Fig. 9b, e, and f). The stress–strain response was stretched to longer deformation values when the crimped yarns were oriented along the load direction.

For a quantitative comparison, the stress–strain response parameters were evaluated according to the definitions given in Fig. 1 ([16,40]). The cracking stress and corresponding strain of the composite are represented by σ_1 and, ε_1 respectively, whereas σ_2 and ε_2 represent the stress and strain corresponding to the end of cracking and/or the point of noticeable stiffness change in the stress–strain response, respectively. The ultimate strength is represented by σ_3, and ε_3 is the ultimate strain. E_1 is the pre-cracking modulus (calculated as the slope of the stress–-strain line in Phase 1. Finally, E_3 is defined as the modulus of the third phase, calculated as slope of the line between σ_2, ε_2 and σ_3, ε_3. The parameters are listed in Table 4.

3.3.1. Cracking stress and pre-cracking modulus

Notably, the warping of the TRMs was observed owing to the susceptibility of the mortar to shrinkage. [16] showed that the curve of TRMs influenced the first phase of the stress–strain response, which was partly adjusted with the average of the deformations calculated on the two faces of the specimen.

Fig. 10. shows the average cracking stress (σ_1) and the pre-cracking stiffness (E_1) of the studied composites. A relatively large scatter was observed in E_1 owing to the impact of the shrinkage-led curvature on both the cracking stress and strain. In Fig. 10(a), the horizontal solid line shows the calculated average tensile strength of the mortar using *FIB Model Code 2010*, and the dotted lines mark the 1 standard deviation threshold.

The average cracking stresses of T1W, T2W, TunW, and TsiW were 53.15%. 65.26%. 56.32% and 106.94% of the calculated tensile strength

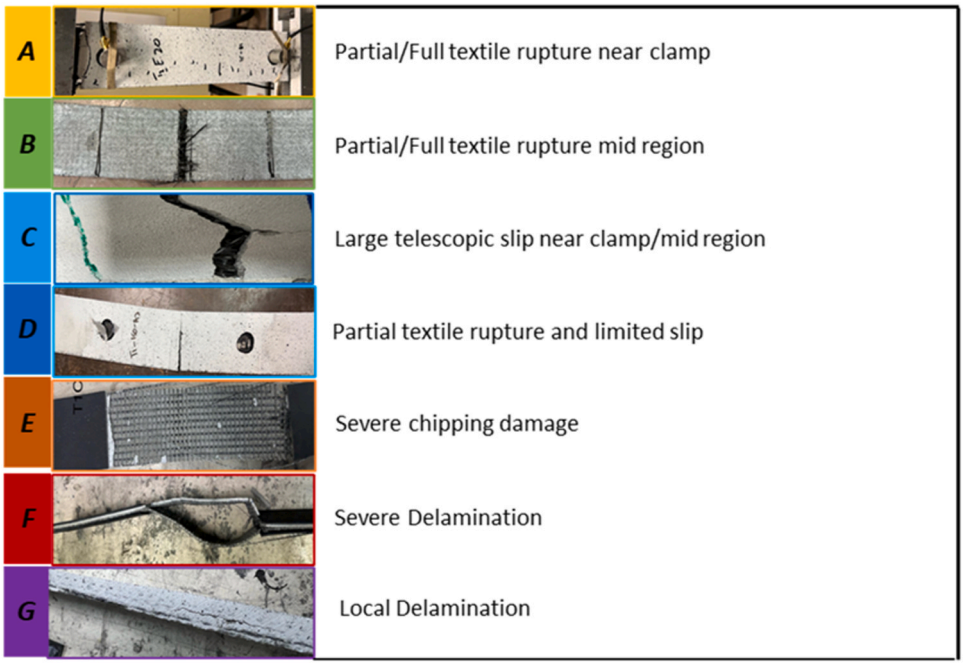

Fig. 6. Classification of the observed failure modes.

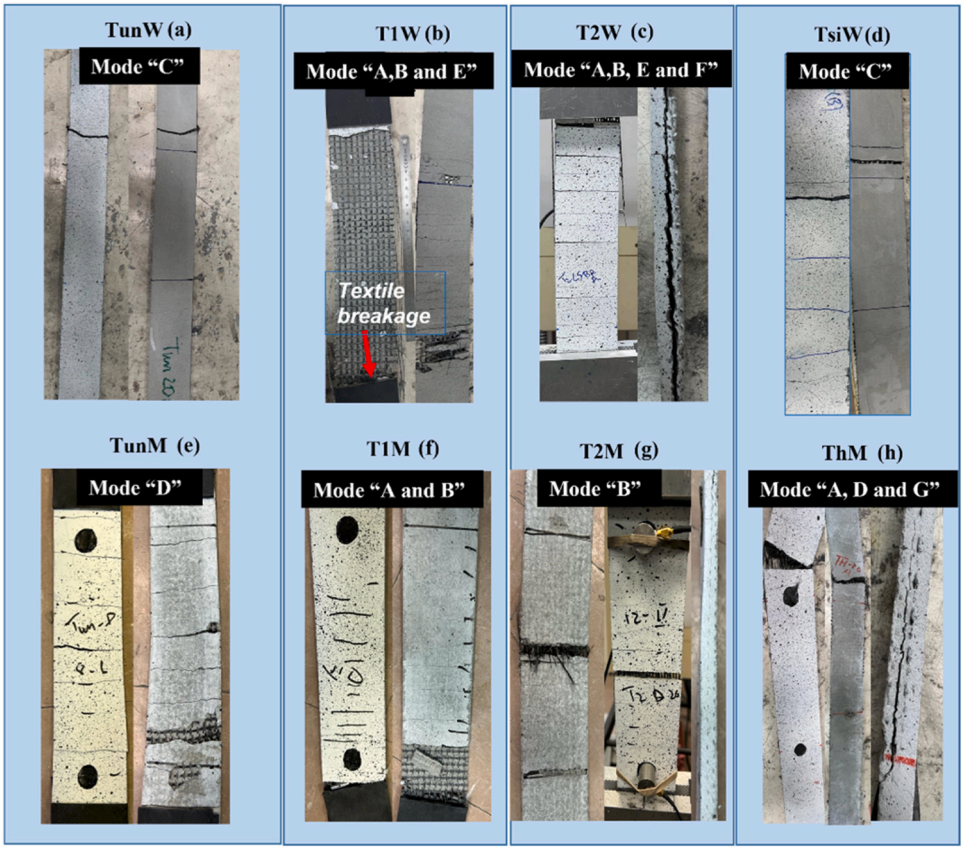

Fig. 7. Failure modes of the tested TRMs: (a) TunW, (b) T1W, (c) T2W, (d) TsiW, (e) TunM, (f) T1M, (g) T2M, and (h) ThM.

of the mortar, respectively. In contrast, T1M, T2M, TunM, and ThM exhibited cracking stresses of 101.2%, 93.8%, 70.8%, and 87.6% of the mortar's strength, respectively.

The higher cracking stress of TsiW can be attributed to the dispersion of microsilica particles from the textile to the mortar, resulting in a denser microstructure and improved cracking stress performance. Except for T1W, in accordance with [26], the coated textile-based composites exhibited a higher average cracking stress than their uncoated counterparts. However, based on the observed scatter, an overlap between the cracking stresses of T1M with TunM and those of T1W with

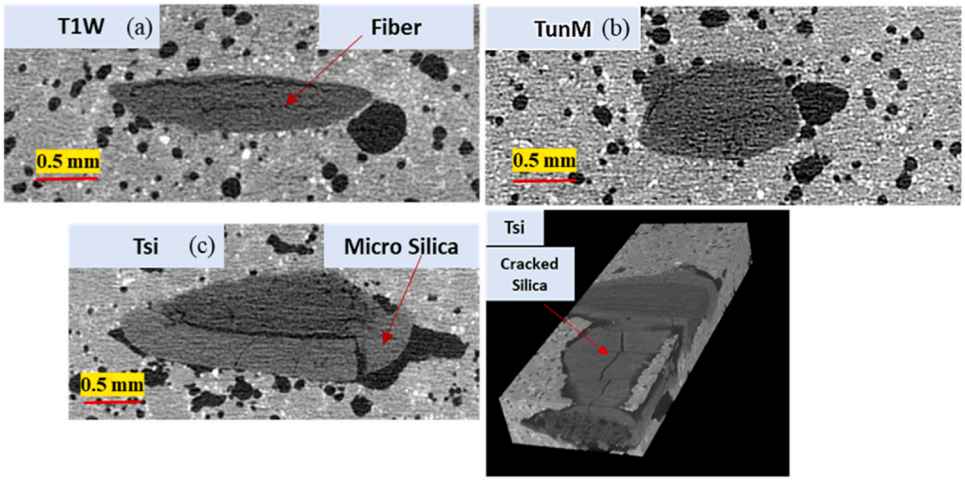

Fig. 8. Description of the integrity of various mortar–textile interfaces. (a) T1W, (b) TunM, and (TsiW).

TunW was observed.

Additionally, the one- and two-layer warp-oriented TRMs (T1M and T2M) exhibited enhanced cracking stress compared with the corresponding weft TRMs. This could have been induced by the 'global' modified shrinkage control, rooted in the altered textile mortar interlock, when the out-of-plane crimp is introduced in the transverse orientation of the specimen. Shrinkage control (although induced by short-fibre inclusions) has been associated with increased cracking stress [41–43]. For T1W and T2W, the direct pull on the out-of-plane crimp in the weft direction may have resulted in a lower cracking stress because of its adverse influence as a discontinuity or weakness along the load direction. For TunM and TunW, the influence of the crimp and/or textile orientation remained within the observed variance in their cracking stress. The pre-cracking modulus was observed to have a larger scatter and fluctuated across different TRM configurations. These fluctuations can be attributed to the influence of mortar shrinkage on both the cracking stress and the corresponding cracking strain.

3.3.2. *Strain contribution of the second phase*

With the exception of T2W, the stiffness in the second phase did not significantly contribute to the overall response. For T2W, a noticeable improvement in the stress was recorded in the second phase. However, in this study, the TRMs exhibited significantly varying behaviours in terms of strain contributions in the second phase. The average strain difference $(\varepsilon_2 - \varepsilon_1)$ was used to evaluate the contribution of the second phase to the overall response (Fig. 11). The largest value of $(\varepsilon_2 - \varepsilon_1)$ was observed for T1W (1.091), followed by TunM (1.06). As reported in [21], multiple layers are associated with a swift cracking process, resulting in a lower deformation. This influence of the number of textile layers was validated for ThM and T2W, with a shorter cracking phase compared with TunM and T1W, respectively. However, no significant difference in $(\varepsilon_2 - \varepsilon_1)$ was observed for T1M and T2M. The effect of the silica coating on the average stretching of the second phase remained within the range recorded for TunW.

The ratios of $(\varepsilon_2 - \varepsilon_1)$ for TunM to TunW and T1W to T1M were 4.8 and 6.4, respectively. Similar trends were observed for T2M and T2W. The larger stretch of the cracking phase (second phase) for TunM and T1W was due to the placement of crimped yarns parallel to the load direction. In addition to straightening of the crimp, a delay in the stable redistribution of stresses led to longer hardening phases. The interruption in the stable stress redistribution can be attributed to the alternating interlock and damage caused by the nature of the crimp.

3.3.3. *third phase parameters*

Fig. 12(a) shows the average ultimate strengths of the tested composites. On average, TsiW exhibited a slightly lower ultimate stress than TunW. The polymer coating was associated with a significant improvement in the ultimate strength. Compared with TunM and TunW, T1M and T1W had 94% and 188% improvements in ultimate strength, respectively. As explained in [27], polymer coating enhances the uniformity of the stress distribution on the yarn cross-section and improves the ultimate performance.

Although not proportionally, a higher number of textile layers has been associated with a higher ultimate strength [18]. Similar global trends were observed in this study. The ultimate strength of T2M was 1.43 times of T1M, whereas ThM exhibited 1.24 times higher peak strength than TunM but 0.63 times than that of T1M. For ThM, the inclusion of the TCSBR layer had a slight influence on the improvement in the strength relative to that of TunM. This can be explained by the larger deformations induced by the slipping of the uncoated textile layers, which led to higher strains on the surfacial zones of the coated yarns, resulting in telescopic cum rupture mode of failure of the coated yarns.

Counterintuitively, T2W resulted in lower strength compared with T1W; however, this behaviour may have resulted from the nonuniform stress on the T2W cross-section due to misalignment and/or bearing damage in the clamp. A more plausible explanation is that a higher number of textile layers shifted the failure mode (as observed for T2W in Fig. 7c), which prevented the full utilisation of the textile, thereby reducing the peak strength [15,21].

The effect of textile orientation on strength was noticeable only for one-layer TCSBR-based composites, with the ultimate stress of T1W being 1.6 times that of T1M. This can be explained by the possible difference in the effectiveness of the mortar–textile interlocking mechanisms associated with crimped yarns. Additionally, a superior load-bearing capacity of the weft orientation was also reported in [30]. According to [30], the flatness of the weft yarns created a larger mortar-to-textile contact surface along with increased penetration of the matrix in flatter weft yarns compared with round warp yarns. This phenomenon resulted in a higher bearing capacity of the weft TRM despite the larger strength of the warp yarns. The absence of this strength improvement in T2W compared with T2M was due to the observed delamination in T2W. It is worth mentioning that the influences of the textile crimp and orientation on the ultimate strength were not identical when uncoated textiles or multiple textile layers were used. First, this indicates the different effectiveness of the mortar–textile bonding in the crimped coated and uncoated yarns and the superseding influence of the failure mode shift in multilayer TRMs. The last-phase modulus (E_3) exhibited trends identical to those observed for the ultimate stress. However, the E_3 value of TsiW was based on that of TsiW-C, which was the only TsiW sample with a distinct linear third phase.

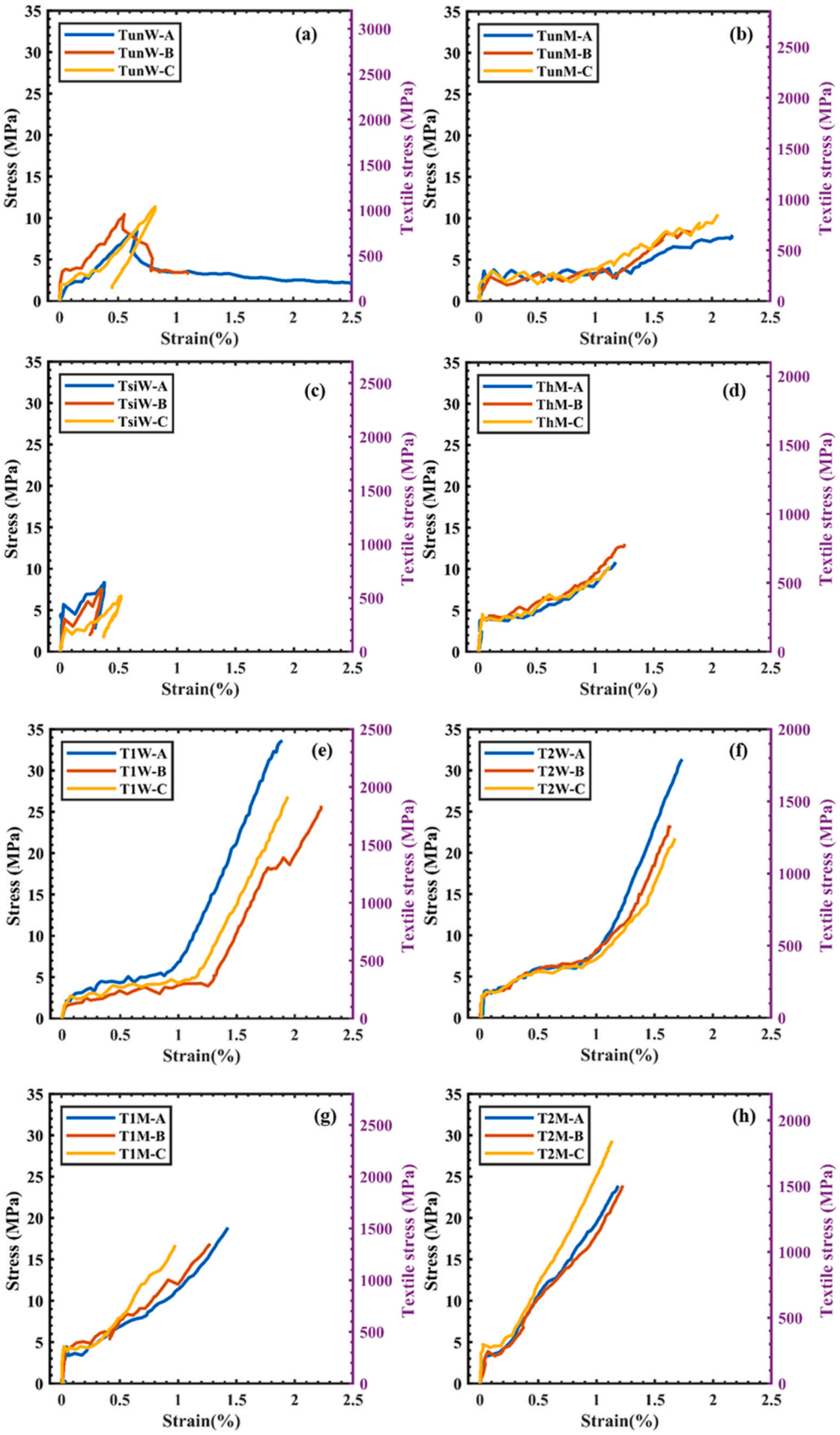

Fig. 9. Experimental stress–strain response of TRMs; (a) TunW, (b) TunM, (c) TsiW, (d) ThM, (e) T1W, (f) T2W, (g) T1M, and (h) T2M.

Table 4
Parameters of the observed stress–strain response.

	ε_1 (%)	σ_1 (MPa)	ε_2 (%)	σ_2 (MPa)	ε_3 (%)	σ_3 (MPa)	E_1 (MPa)	E_3 (MPa)	Toughness (MPa)
T1W	0.048	2.30	0.95	5.97	1.89	33.42	4744.89	2919.81	21.96
	0.046	1.90	1.28	4.50	2.25	25.44	4136.51	2172.36	19.40
	0.041	2.24	1.17	5.18	1.94	26.63	5501.22	2774.70	16.45
Average (CoV)	0.044 (7.16%)	2.14 (8.21%)	1.135 (12.17%)	5.21 (11.51%)	2.028 (7.76%)	28.49 (12.32%)	4794.2 (11.6%)	2622.2 (12.3%)	19.27(11.6%)
T2W	0.043	3.27	0.96	7.50	1.75	31.93	7534.77	3122.11	19.64
	0.018	2.00	0.93	7.24	1.65	23.94	11,222.17	2320.27	15.01
	0.020	2.62	0.95	6.72	1.68	22.00	9042.91	2074.60	14.31
Average (CoV)	0.026 (34.75%)	2.63 (19.62%)	0.947 (1.32%)	7.15 (4.5%)	1.694 (2.29%)	25.95 (16.54%)	9266.6 (16.3%)	2505.66 (17.8%)	16.3 (14.4%)
TsiW	0.029	5.89	0.29	6.65	0.38	8.70	20,290.08		2.34
	0.036	3.98	0.28	5.75	0.36	7.59	10,960.79		1.69
	0.045	3.09	0.31	3.81	0.52	7.01	6878.07	1540.86	2.02
Average (CoV)	0.036 (17.68%)	4.31 (27.05%)	0.292 (5.40%)	5.40 (21.90%)	0.420 (16.99%)	7.76 (9.02%)	12,709 (44.1%)	1540.86	2.01 (13.2%)
TunW	0.071	1.93	0.25	2.90	0.66	8.52	2709.83	1359.26	2.88
	0.014	2.64	0.19	4.11	0.56	10.38	18,604.83	1733.40	3.32
	0.016	2.25	0.33	3.25	0.82	10.74	14,315.28	1532.18	4.32
Average (CoV)	0.033 (78.63%)	2.27 (12.77%)	0.257 (21.81%)	3.41 (14.91%)	0.679 (15.97%)	9.88 (9.87%)	11,876.65 (56. %)	1541.61 (9.9%)	3.5 (13%)
T1M	0.099	3.8	0.2	3.82	1.43	19.27	3838.38	1256.09	13.46
	0.039	3.9	0.25	4.9	1.27	17.22	10,000	1207.84	11.77
	0.05	4.6	0.25	4.1	0.98	17.05	9200	1773.97	8.65
Average (CoV)	0.062 (41%)	4.1 (8.6%)	0.233 (10.10%)	4.27 (10.7%)	1.226 (15.1%)	17.84 (5.6%)	7679.4 (35.6%)	1412.63 (18.1%)	11.29 (17.6%)
T2M	0.052	3.26	0.18	3.83	1.19	23.84	6269.23	1981.18	14.34
	0.07	3.89	0.22	4.55	1.24	24.32	5557.14	1938.23	14.96
	0.031	4.48	0.27	5.73	1.13	28.69	14,451.61	2669.76	15.69
Average (CoV)	0.051 (31%)	3.87 (12.8%)	0.22 (16.4%)	4.70 (16.6%)	1.18 (3.8%)	25.61 (8.5%)	8759.3 (46.07%)	2196.37 (15.2%)	14.99 (3.6%)
TunM	0.047	3.81	1.32	3.99	2.2	8.76	8106.38	542.04	10.5
	0.035	1.15	1.2	3.02	1.81	8.21	3285.71	850.81	6.99
	0.12	3.67	0.87	3.02	2.06	10.5	3058.33	628.57	10.61
Average (CoV)	0.067 (55.7%)	2.87 (42%)	1.13 (16.8%)	3.34 (13.6%)	2.02 (7.9%)	9.15 (10.6%)	4816.8 (48.3%)	673.8 (19.3%)	9.36 (17.9%)
ThM	0.028	2.54	0.38	4.05	1.18	10.77	9071.42	840	6.89
	0.026	3.8	0.27	4.49	1.25	13.2	14,615.38	888.77	9.09
	0.038	4.33	0.46	4.61	1.12	10.11	11,394.73	833.33	6.62
Average (CoV)	0.030 (17.11%)	3.55 (21.1%)	0.37 (21.05%)	4.38 (5.49%)	1.18 (4.48%)	11.36 (11.7%)	11,693.8 (19.1%)	854.03 (2.89%)	7.53 (14.6%)

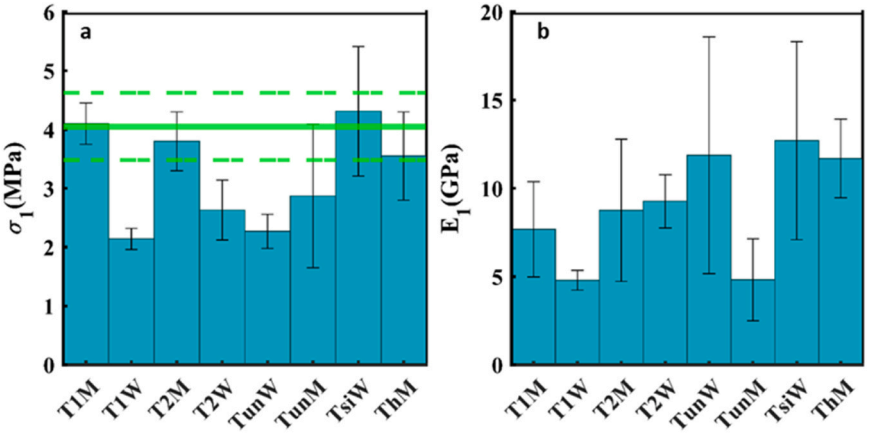

Fig. 10. Cracking stress for the studied TRMs (a), First phase modulus (b).

The ultimate strains (ε_3) for T1M, T2M, TunM, and ThM were 1.22%, 1.18%, 2.02%, 1.18% and 1.18%, respectively (Fig. 13(a)). Correspondingly, 2.02%, 1.69%, 0.67% and 0.42% (ε_3) was recorded for T1W, T2W, TunW and TsiW. The sensitivity of the ultimate strain to the textile crimp preceded that of the polymer coating. The higher value of (ε_3) in TunM was due to the deformations contributed by straightening of the in-plane crimp, and its influence was identically reduced in ThM when a layer of TCSBR was added. Similarly, T1W exhibited the highest ultimate strain in the weft direction. Note that TunM, with an in-plane crimp, and the TCSBR-based T1W, with an out-of-plane crimp, exhibited identical average ultimate strains. Similar influence of crimp was observed for T2M and T2W.

For T2M, the number of layers had a marginal effect on the average ultimate strain reduction. However, a reduction of 19.5% was observed for T2W relative to T1W owing to the alteration of the failure mode (Fig. 7b and c). TsiW had the lowest ultimate strain owing to ineffective

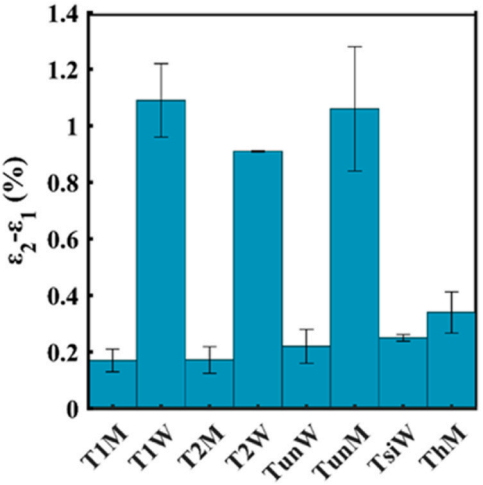

Fig. 11. Extent of deformation observed in the second phase of the stress–-strain response.

stress transfer at the textile-mortar interface and poor adhesion.

Fig. 13b represents the deformation capacity (ductility) factor of the third phase, calculated as the ratio of $\varepsilon_3 to \varepsilon_2$. For the TCSBR-based TRMs, the effect of the crimp on the (ductility) factor was significant, but no apparent influence of the two layers was observed. Additionally, it is worth noting that for TunM and T1W the average $\varepsilon_3/\varepsilon_2$ factors were identical within 2%. The inclusion of crimp in the load direction resulted in decrease in $\varepsilon_3/\varepsilon_2$, with 66% reduction for T1W compared with T1M and 30% decrease for TunM compared with TunW. Thus, the inclusion of the out-of-plane crimp led to larger reduction in $\varepsilon_3/\varepsilon_2$ compared with the reductions observed for in plane crimp.

The comparison of load oriented crimped yarn TRMs (T1W, T2W, and TunM) showed that $\varepsilon_3/\varepsilon_2$ was insensitive to the polymer coating. In contrast, the load aligned non-crimped yarn TRMs (T1M, T2M, and TunW) showed that TCSBR-based TRMs had higher $\varepsilon_3/\varepsilon_2$ than $T_{uncoated}$ textile-based TRMs. However, this explanation is based on the assumption of insensitivity of the $\varepsilon_3/\varepsilon_2$ factor to textile orientation.

The third phase deformation capacity of TsiW was reduced by 46% compared with that of TunW. For ThM, the inclusion of the TCSBR layer resulted in 83% increase in $\varepsilon_3/\varepsilon_2$ relative to TunM. ThM had both lower $\varepsilon_3 and \varepsilon_2$ values than TunM; however, its influence on reduction of ε_2 was more paramount, as demonstrated by increase in $\varepsilon_3/\varepsilon_2$.

3.4. Toughness

The variation in the average toughness (area under the stress–strain curve) with the strain for the studied TRMs is shown in Fig. 14. The corresponding stress–strain curve is also plotted in the same figure. The shaded regions under the toughness–strain curve separate the contributions of each phase. Each shaded area represents the toughness–strain product, and the height of the shaded region (along the ordinate) indicates the toughness value.

The variation in toughness with strain was nonlinear. In the presence of a crimp and/or polymer coating, the toughness was distributed relatively at larger strains. The placement of crimped yarns parallel to

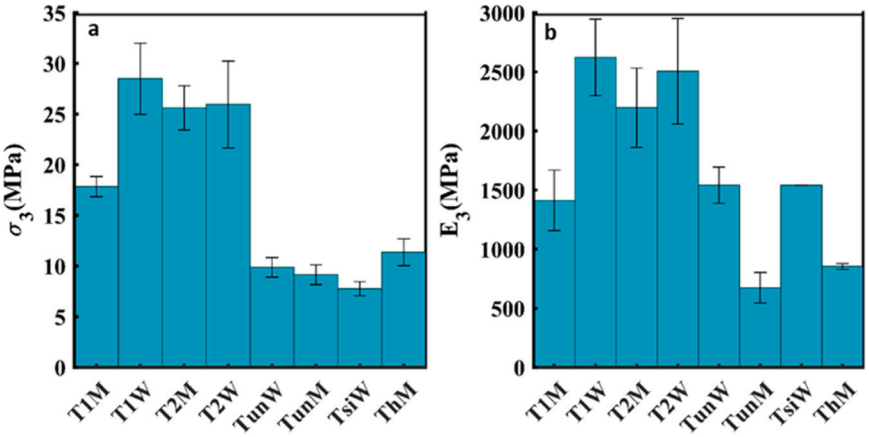

Fig. 12. Ultimate strength (a) and last-phase modulus (b) of the studied TRMs.

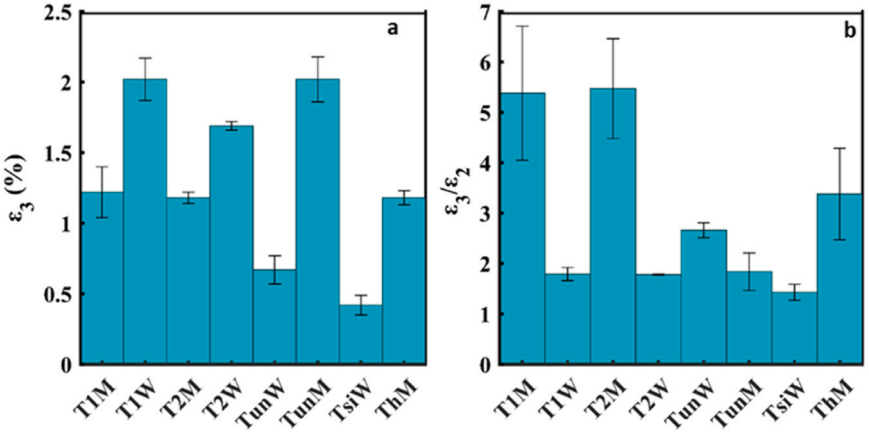

Fig. 13. Ultimate strain (a) and the third phase strain contribution factor of TRMs (b).

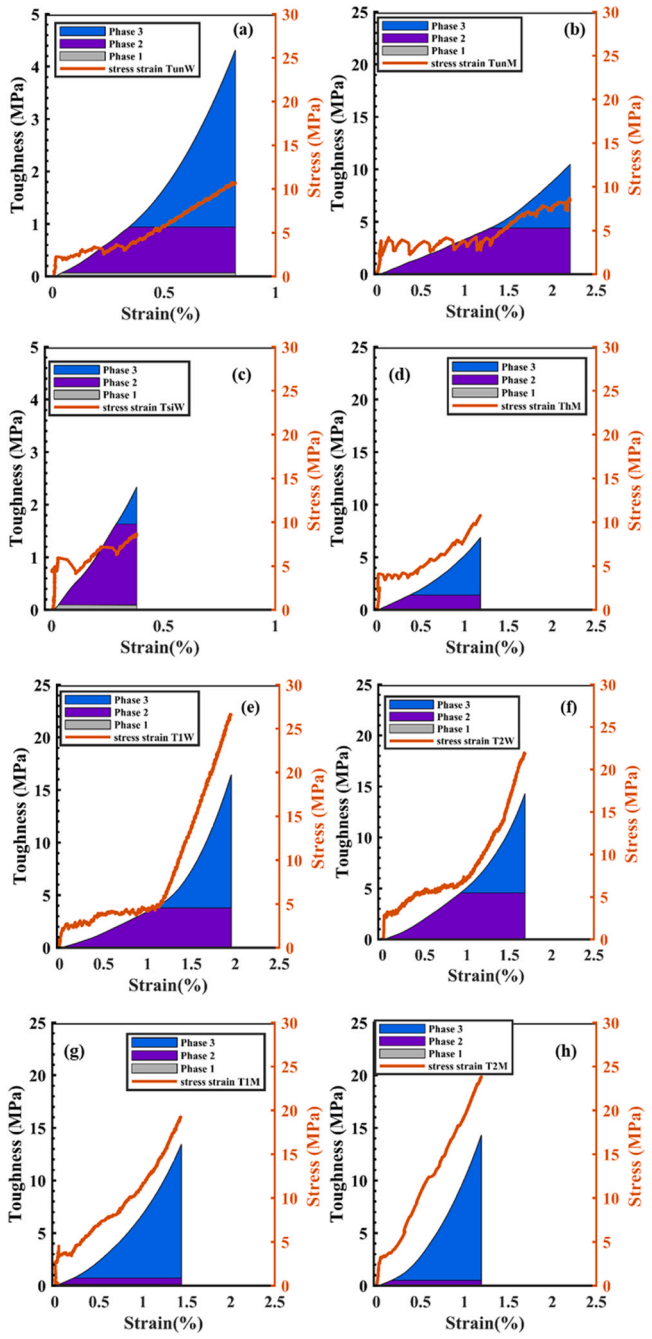

Fig. 14. Variation in toughness with strain for a representative stress–strain response of TRMs; (a) TunW, (b) TunM, (c) TsiW, (d) ThM, (e) T1W, (f) T2W, (g) T1M, and (h) T2M.

the load, irrespective of the textile coating, resulted in a higher toughness than their uncrimped counterparts. The application of microsilica resulted in a 42% decrease in total toughness compared with that of TunW. The number of layers had a marginal effect on the total toughness because of sensitivity to the observed failure mode. T2M exhibited a 20.5% enhancement in the total toughness compared with that of T1M. However, T2W showed an 18.1% reduction compared with T1W. The higher toughness of TunM was attributed to its ability to sustain larger strains. Compared with TunM, the inclusion of a TCSBR layer in ThM reduced the toughness by approximately 20%.

Fig. 15 shows that, on average, the major percentage contribution to toughness was by the third phase except for TsiW, where the response was dominantly biphasic. The contribution of the pre cracking phase to the toughness was relatively negligible.

3.5. Displacement fields and cracking behaviour

Fig. 16 shows the normalised vertical displacement (normalised with the displacement at the peak load) for the representative case of the studied TRMs, plotted at 50% of the peak load P_{ult}. In the observed region of interest (Fig. 4), the data points from DIC were used to fit a surface using scattered 2-D linear interpolation [44]. The jumps along the displacement represent the crack opening displacement (COD). The distance between jumps (along the length) denotes the crack spacing [8]. Globally, with an increase in crack density, a reduction in the COD was observed.

3.5.1. Crack spacing

Fig. 17 shows the representative normalised crack spacing (*Cs*) evolution plotted over the stress–strain response based on the DIC. The average number of cracks (for three samples) observed at the end of the test is shown in Fig. 17**.** The crack spacing was calculated by dividing the length between the clamps/gauge length by (n + 1), where n is the number of cracks. The computed crack spacing was normalised using the observed length of the TRM**.**

The crack spacing reduction showed that in some cases (where the TCSBR was used), cracking continued into the stiffer phase (third) of the response [16,45].

Both coating modification and textile orientation and/or crimp influenced the cracking behaviour. The largest crack spacing was observed for TsiW (Fig. 17c). Unlike microsilica, the polymer coating significantly reduced the crack spacing in T1W (Fig. 17e) compared with that of TunW (Fig. 17a). However, TunM exhibited a higher number of cracks than TunW, which demonstrated that the presence of in-plane crimped yarns in the load direction led to a higher number of cracks than when the crimp was placed in the transverse direction. With respect to the effect of orientation and crimp on the TCSBR-based composites, T1W and T2W had more cracks than T1M and T2M, respectively. This may have been caused by the presence of 1) an out-of-plane crimp and/or 2) enhanced bonding of the flatter weft yarns [30].

The cracking behaviours of T1W and T2W associated with the second phase of the stress–strain response can be classified into two different stages**.** The case of T2W in Fig. 17 g is used to elaborate on the different segments (see a-b, b-c, and c-d in Fig. 17g).

- Zone 1: First cracking segment (a-b), where the cracking stress of the mortar was exceeded

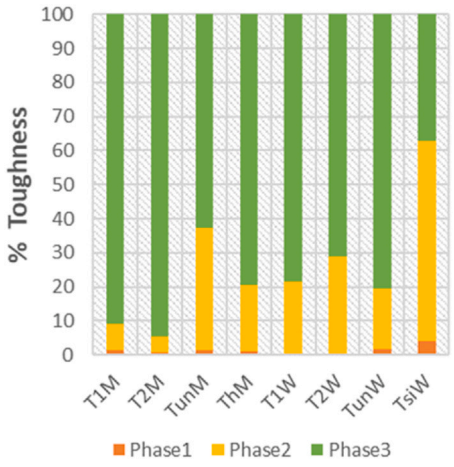

Fig. 15. Percentage contribution of each phase to the toughness.

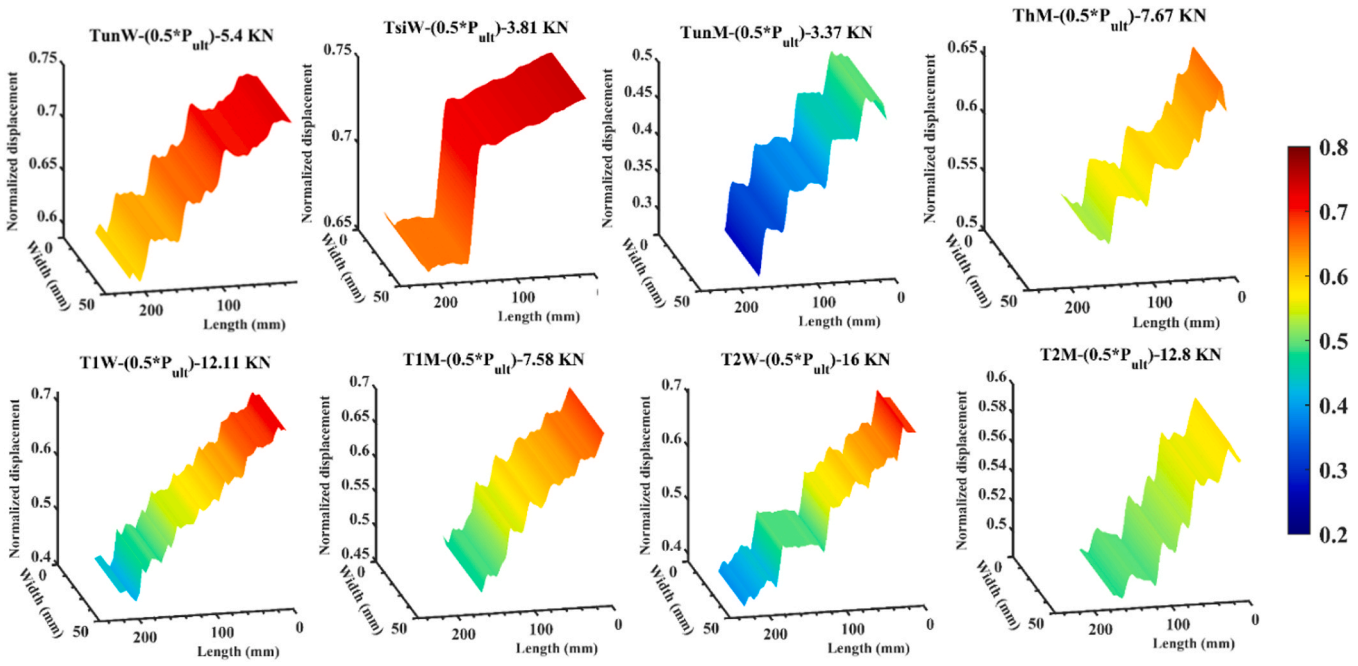

Fig. 16. Displacement fields from DIC at 50% of the ultimate load.

- Zone 2: The second segment (c-d), where denser microcracking was initiated by pull on the transversal yarns owing to the stretching of the textile in the pre-established cracks (as shown in Fig. 17).

The two zones were often separated by a lag (b-c) in the crack-spacing reduction (T1W and T2W), but not necessarily as there might have been cracking during the lag (T2W in Fig. 17g). The lag phase was associated with chipping damage at approximately every transverse yarn distance (see in failure modes Fig. 7b). Note that, particularly for T2W, the end of Zone 1 marked the take-off of stiffness, which can be explained by the established stretch on the textile bridging the formed cracks. Globally, the delay in stiffness take-off with the associated lag in cracking (T1W and T2W) can be attributed to the subsequent anchoring and release of the out-of-plane crimp of the weft yarns. Fig. 18.

3.5.2. Crack opening displacement (COD)

The evolution of the COD with stress was obtained using MatchID (Fig. 19). For T1W and T2W, the COD was noticeably influenced by the position of the crack, time of appearance, and density of cracking.

For T1W and T2W, the COD–stress behaviour can be idealised by bilinear behaviour: 1) rapid crack widening and 2) a mild crack opening stage. While for T1M and T2M, a linear idealization can be adopted. The presence of bilinear behaviour for T1W and T2W resulted from the initially higher crack-opening rate owing to the straightening of the crimp.

For TunM, the combined influence of the crimped yarns and the ineffectiveness of the filament-to-filament interaction of the uncoated yarns led to larger slips and COD values. Unlike the TCSBR-based TRMs, the crack formation in TunM was associated with identifiable stress drops. This points towards the stiffer function of the polymer-coated textile during crack formation. Similar behaviour was observed for ThM, where the inclusion of a coated textile layer significantly reduced the extent of stress drops and the peak COD.

For both TunW and TsiW, the cracks at telescopic slip were not included in the analysis. Slips in some specimens occurred at or near the clamps, which prevented the exploitation of the DIC results at that particular location. These cracks ranged between 3.5 and 4 mm in width, when manually measured after the test. For the other cracks, Fig. 19a and c illustrate the COD–stress relation for TunW and TsiW, respectively. Here, the COD–stress response comprised four distinct stages: 1) abrupt opening of the crack, 2) stress drop (owing to redistribution), 3) followed by increase in COD until peak stress, and 4) reduction in COD as post-peak stress decreased with the progression of telescopic slip. The maximum COD at the peak stress can be considered an apparent value, as the decrease in stress led to a reduction in COD. The test was stopped at different instances with at least 70% reduction in the peak stress. The idealised behaviour of the COD–stress for TsiW and TunW is shown in Fig. 20. Theoretically, the residual value of COD at zero stress can be obtained through linear extrapolation of the post-peak COD–stress relationship, which will be interesting for the serviceability limit state to identify the extent of crack closure with the stress removal.

$$COD - COD_f = \frac{COD_p - COD_f}{\sigma_p - \sigma_f}\left(\sigma - \sigma_f\right) \tag{1}$$

$$COD = \frac{COD_p - COD_f}{\sigma_p - \sigma_f}\left(\sigma - \sigma_f\right) + COD_f \tag{2}$$

$$[for \quad \sigma = 0, COD = COD_R] COD_R = \left(-\sigma_f\right)\frac{COD_p - COD_f}{\sigma_p - \sigma_f} + COD_f \tag{3}$$

where σ_p, COD_p *represents the values at peak and* σ_f, COD_f *denotes the values at the end of the test*

3.5.2.1. Peak COD. Fig. 21 shows the average peak COD values for the tested composites along with the corresponding ultimate stresses. Owing to the influence of progressive filament rupture at various cracks, the largest scatter in the average COD was observed for TunM, followed by T2W and ThM, where delamination may have influenced the relative opening of the cracks [34]. The highest average COD at the lowest stress was recorded for TunM owing to the presence of crimped yarns in the load direction. This influence of the crimp was not visible for T1W and T2W. The higher crack density in T1W and T2W led to lower crack openings than in T1M.

The effectiveness of the polymer coating in controlling the crack width was evident, and a significantly large stress was required to reach higher COD values. Moreover, the use of a silica coating resulted in an increase in the average COD owing to the compromised textile–mortar interface. Finally, increasing the number of textile layers did not

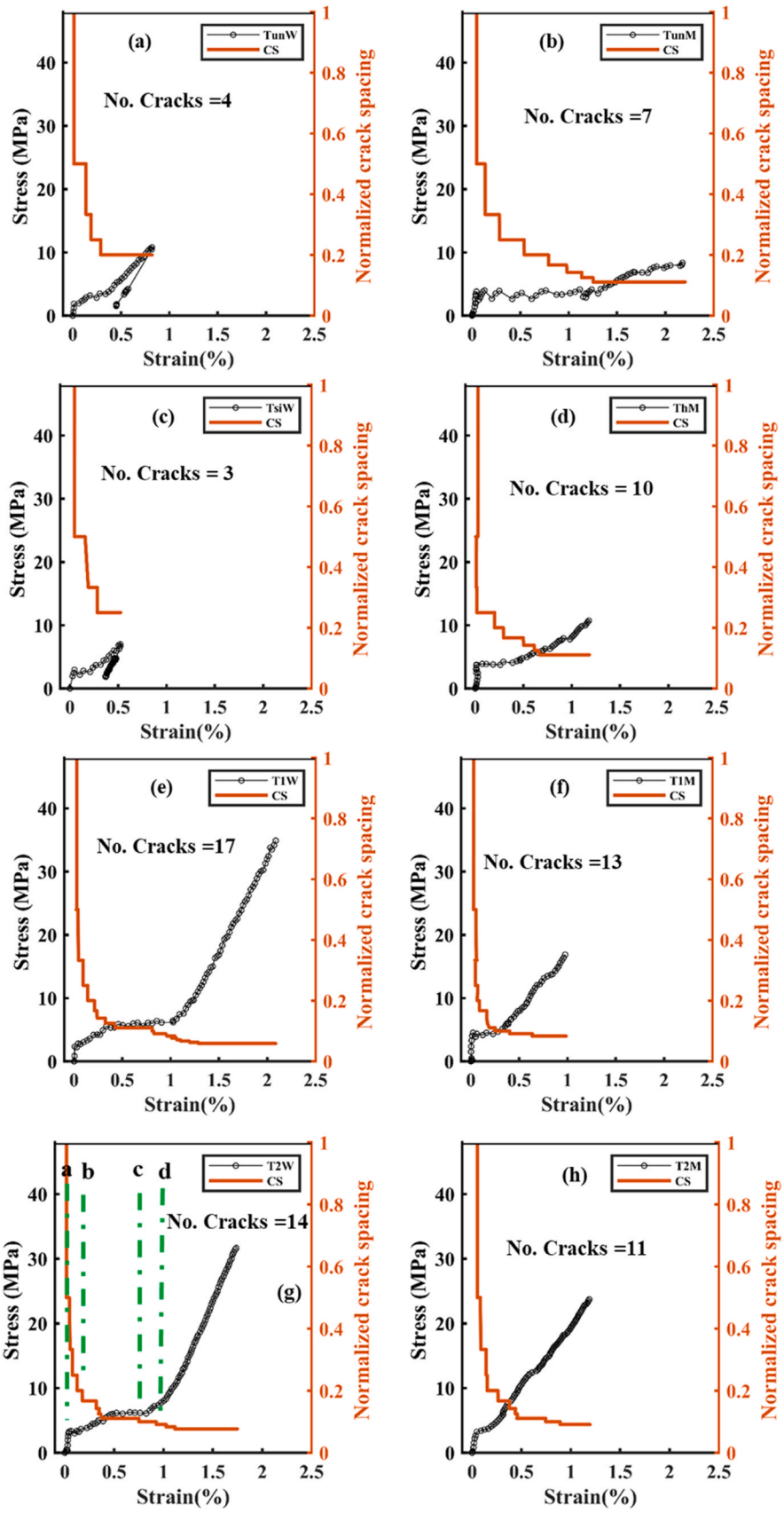

Fig. 17. Crack spacing evolution and the corresponding stress–strain response of TRMs; (a) TunW, (b) TunM, (c) TsiW, (d) ThM, (e) T1W, (f) T2W, (g) T1M, and (h) T2M.

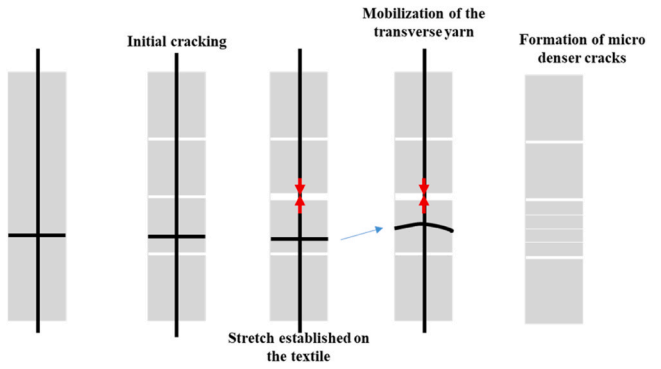

Fig. 18. Schematic representation of the crack evolution in T1W and T2W.

guarantee a reduction in the average COD owing to the risk of delamination.

3.5.2.2. COD–stress drop. Unlike the TCSBR-based TRMs, the formation of cracks in TsiW, TunW, and TunM was associated with identifiable stress drops. The magnitude of the stress drop exhibited direct correlation with COD_p (crack opening at the peak stress, where 'p' signifies peak/ultimate stress) for TsiW and TunM. while indirect correlation was observed with TunW (Fig. 22). This contradictory behaviour may be related to the observed magnitude of the stress drop. For TunW, the stress drop varied in the range 0.15–0.5 MPa, and for TsiW and TunM, the stress drop fluctuated in the range 0.40–2.04 MPa. The estimation of COD_p could provide an estimate of the largest possible COD observed at the peak stress, excluding the cracks where telescopic failure was recorded for TsiW and TunW. Note that the stress drops can be easily identified through the force-time signal. The R^2 value for the TunM vs. the stress drop fit was 0.4. For TunM, the scatter can be explained by a) the nature of the progressive filaments/yarn ruptures which accelerated the crack opening (Fig. 19b), and 2) the relative anchoring and straightening of loaded in-plane crimped yarns. Further studies are required to enhance our understanding of the relationship between COD and stress reduction. This understanding will provide a basis for better control of crack openings by managing the redistribution of effort to textiles. Maintaining smaller crack openings in TRMs is crucial for durability, particularly when TRMs are used to strengthen RC structures.

3.6. Analytical modelling

The ACK theory in [46,47] has been used to simulate the triphasic behaviour of the TRMs under uniaxial tension [48]. The three phases are modelled using the material properties of the textile and mortar, as discussed further:

The first phase is calculated till the cracking strength σ_1 of the composite is reached.

$$\sigma_1 = V_m \sigma_m \tag{4}$$

The pre-cracking modulus is given by

$$E_1 = V_f E_f + V_m E_m \tag{5}$$

In Eq. (5) V_m and V_f represent the matrix and reinforcement ratios, respectively. E_f and E_m are the moduli of the textile and matrix, respectively. σ_m is the direct tensile strength of the matrix.

According to the ACK, no increase in stress is associated with the second phase, i.e. $\sigma_1 = \sigma_2$. The corresponding strain (ε_2) at the end of second phase is given by

$$\varepsilon_2 = \left(1 + 0.666 * \frac{V_m E_m}{V_f E_f}\right) * \frac{\sigma_m}{E_m} \tag{5}$$

The third phase ends with the failure by breakage of the reinforcement. The ultimate strength (σ_3) and modulus of the third phase (E_3) are calculated as follows:

$$\sigma_1 = V_f \sigma_f \tag{6}$$

$$E_3 = V_f E_f \tag{7}$$

The results obtained using the ACK model are shown in Fig. 23. Because the failure in $T_{uncoated}$-based TRMs was dominated by the partial rupture and slip of the fibres, a modification factor was used to obtain an improved fit of the model. According to [30], the strength efficiency factor of the textile in the TRM was 0.49. Therefore, σ_3 for TunW, TsiW, TunM, and ThM was multiplied by 0.49. Additionally, the stiffness E_f values for TunM and ThM were also modified by a factor of 0.49. On average, the ACK curves exhibited a good match with the experimental curves of TunW, ThM, T1M, and T2M. For TsiW, the ACK overestimated the strength because no adjustments were made for the compromised interface of TsiW.

3.6.1. Strain modification term

For TunM, T1W, and T2W, the ACK model did not match the experimental data well. From Eq. (5), ε_2 is dependent upon material properties of the matrix and reinforcement, which assume a constant value for a particular case of mortar and textile. However, TunM, T1W, and T2W exhibited longer secondary phases because of the presence of crimped yarns in the load direction. Considering this, an additional term ($\varepsilon_{2,crmp}$) for the modification of $\varepsilon_2$was proposed in this study based upon the geometry of textile.

$$\varepsilon_{2,\mathrm{mod}} = \left(1 + 0.666 * \frac{V_m E_m}{V_f E_f}\right) * \frac{\sigma_m}{E_m} + \left(\varepsilon_{2,crmp}\right) \tag{8}$$

In Fig. 24, the proposed mechanism of crimp straightening that contributes to the additional deformation observed for TunM, T1W, and T2W is presented. The geometry around the crimped yarn was approximated by a triangular region 'abc'. The average height of crimp 'b' was calculated from the tomography, 'a' is half the distance between two transverse yarns, and 'c' is half the curved length of the yarn between two transverse roving. The average value of 'b' for $T_{uncoated}$ was 0.72 and 0.54 mm for TCSBR.

The modification term is based on the following assumptions:

- Complete and uniform straightening of the yarns at cracks. This implies that a uniform crack opening was assumed across the width and thickness of the TRM. Additionally, the intra-filament slip was ignored.
- A linear approximation of the crimped geometry was performed. The maximum crimp was assumed to be located midway between the two transverse rovings.
- The average crimp value was used without considering its stochastic nature.

The additional displacement due to straightening at a single crack was calculated using Eqs. (9) and (10):

$$d_{add} = 2 * (c - a) \tag{9}$$

$$c = \sqrt{a^2 + b^2} \tag{10}$$

The total displacement and strain were obtained using Eqs. (11) and (12), respectively.

$$d_{add,total} = \left(d_{add} * N_{C,2}\right) \tag{11}$$

$$\varepsilon_{2,add} = \frac{d_{add,total}}{L} \tag{12}$$

where $N_{C,2}$ is the number of cracks formed till the end of phase 2, and L is the gage length of the sample.

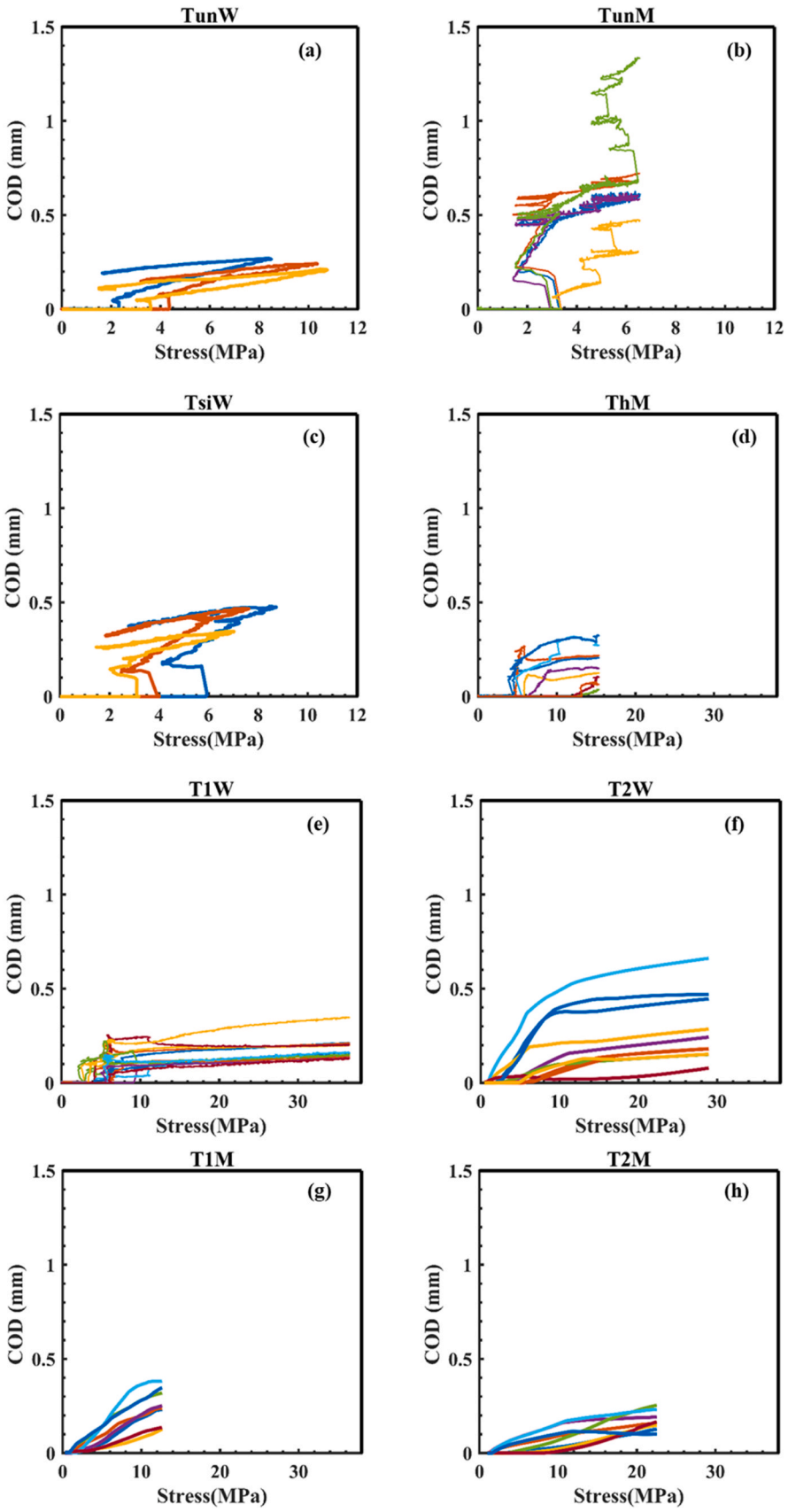

Fig. 19. Evolution of crack opening displacement with stress for TRMs; (a) TunW, (b) TunM, (c) TsiW, (d) ThM, (e) T1W, (f) T2W, (g) T1M, and (h) T2M.

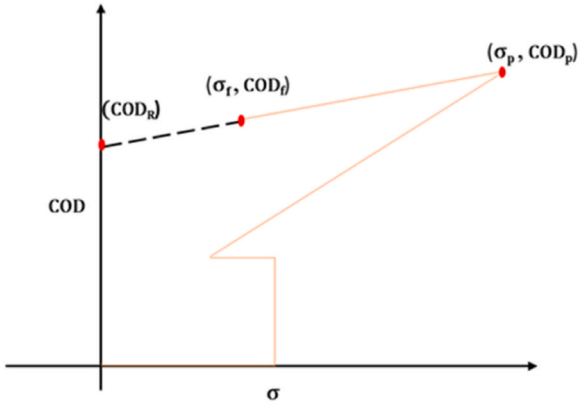

Fig. 20. COD vs Stress idealization for TunW and TsiW.

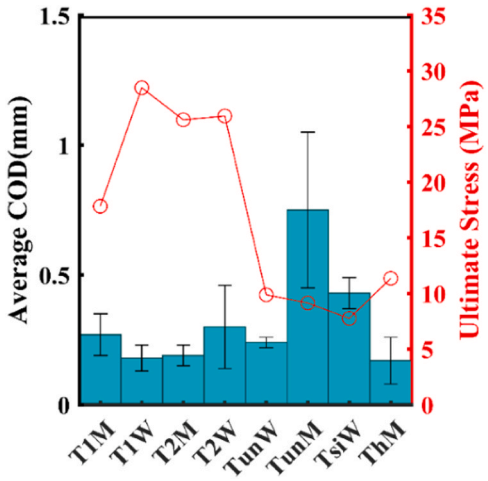

Fig. 21. Average peak COD and the corresponding ultimate stress.

Fig. 23 (for TunM, T1W and T2W) shows that, globally, the proposed modification term provided a good match of the analytical (ACK-MOD) and experimental results. However, for T2W, the stiffening of the second stage could not be simulated based on the ACK assumptions. Additionally, the average T1W strength was underestimated by the model.

The comparison of experimental ε_2 and the modified ACK ε_2 values is shown in Fig. 25. Compared with T2W, T1W and TunM exhibited close approximation of ε_2 to the experimental results within 1 standard deviation. The error bars in Fig. 22 correspond to a standard deviation of 1. From the corresponding error bars, the ACK ε_2 for TunM was overpredicted but within the standard deviation limit. For both T1W and T2W, the ACK ε_2 was underpredicted. A comparison of the difference between the average experimental and modified ACK ε_2 showed that the prediction was off by 15.4%. 10.2%, and 9.7% for T1W, T2W, and TunM, respectively. The respective ε_2 values are shown in Table 5.

The proposed modification term permitted a simple approach to address the deformations contributed by the crimp of the textile. One of the limitations is the requirement for microscale observations for the measurement of the crimp, which can also prove to be sufficiently variable (particularly in the case of uncoated textiles). Further studies can be conducted to relate the crimp to easily measurable properties (like the diameter of the yarns). Finally, the modification term requires information regarding the crack spacing at the end of the second phase of the stress–strain response.

4. Conclusion

This study analysed the influence of crimped textiles on the tensile and cracking responses of textile-reinforced mortar composites. For this purpose, uncoated, SBR, coated and microsilica-modified textiles were used. This study was also extended to assess the influence of the number of coated textile layers and hybrid multilayer textiles (coated and uncoated) on TRMs. Stereo DIC was used to elicit cracking behaviour. Finally, a modified strain term for the second phase of the ACK model was proposed to cater to the crimped geometry of the textile. The following were the main conclusions of this study.

- The stress–strain response of TRMs was sensitive to crimped yarns when oriented in the load direction. Larger deformations were observed due to the straightening of the crimp, irrespective of the number of textile layers adopted (TunM, T1W, and T2W). The deformations were reduced when an uncrimped load-oriented TCSBR layer was placed between two crimped $T_{uncoated}$ textile layers in the ThM. The influence of the textile crimp and/or orientation on the ultimate strength was sensitive to the polymer coating and the number of layers.
- The polymer coating was associated with a significant improvement in the ultimate capacity of TRMs. The manual addition of the microsilica coating resulted in the agglomeration of silica at the textile mortar interface of TsiW. The deposited silica acted as a weak zone, compromising the TRM capacity.
- TCSBR-based one-layer TRMs (T1M and T1W) failed owing to textile rupture. TunM and TunW exhibited partial breakage with textile slip. The adoption of two layers in T2W led to delamination at failure, which was not observed in T2M. The extent of delamination in ThM was less severe than that in T2W.
- The use of load-oriented coated crimped yarns was associated with chipping damage, completely exposing the textile to one of the faces of the TRMs (e.g. T1W).

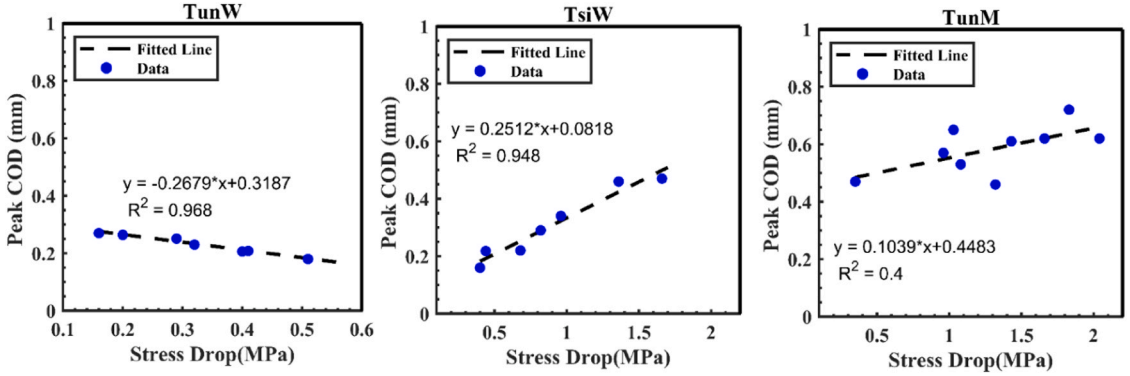

Fig. 22. COD–stress drop relationship for TunW, TsiW, and TunM (left to right).

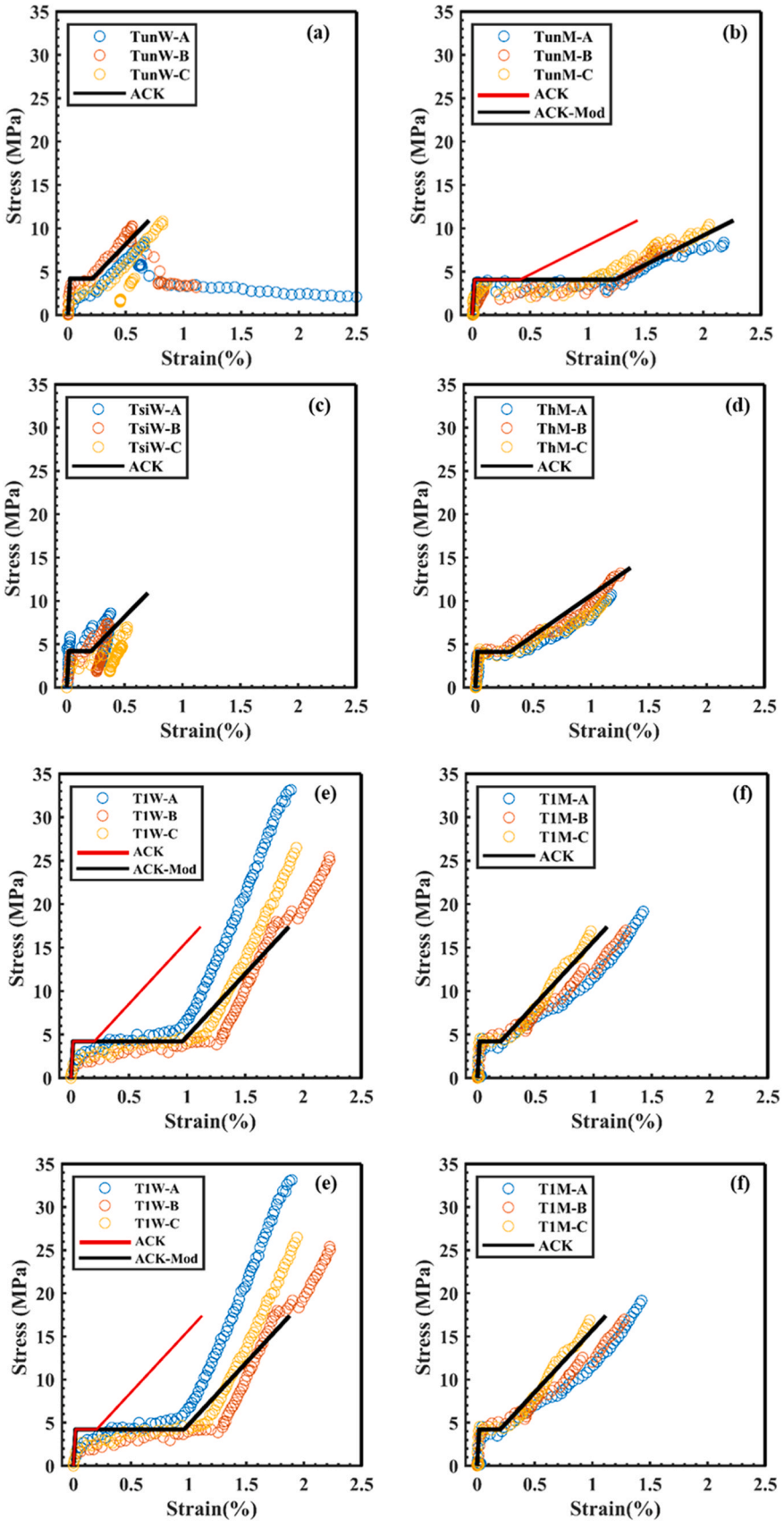

Fig. 23. Experimental and analytical stress–strain response of the TRMs; (a) TunW, (b) TunM, (c) TsiW, (d) ThM, (e) T1W, (f) T2W, (g) T1M, and (h) T2M.

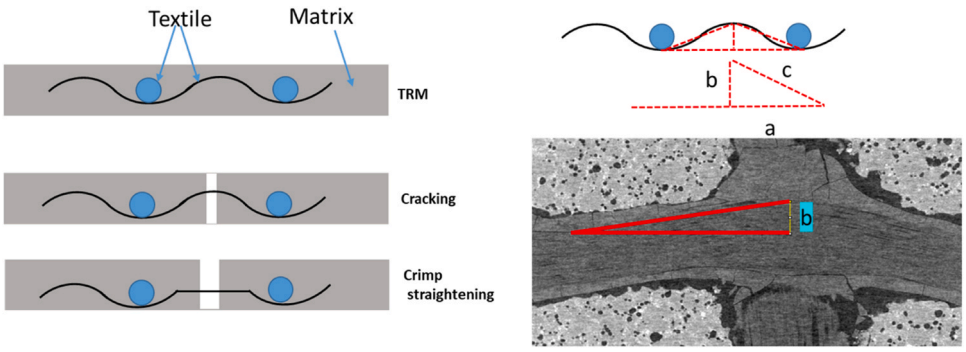

Fig. 24. Crimp straightening in TRMs after cracking.

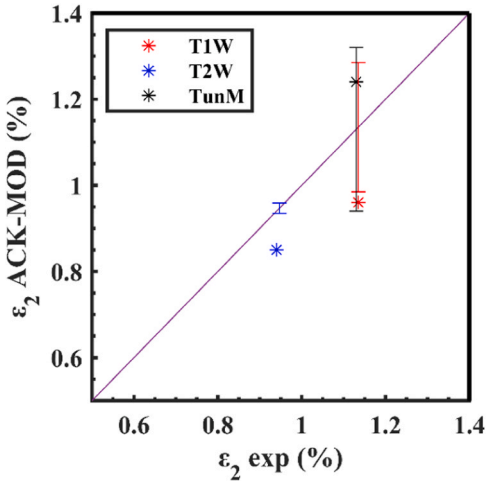

Fig. 25. Comparison of ACK-MOD and experimental ε_2.

Table 5
Second-phase strain predicted and experimental values.

	ε_2 exp (%)	ε_2 ACK-MOD (%)	% Error
T1W	1.135	0.96	15.40%
T2W	0.947	0.85	10.20%
TunM	1.13	1.24	9.70%

- The use of polymer-coated textiles led to the continuation of cracking in the third phase of the stress–strain response. T1W and T2W showed two different zones of cracking in the second phase, separated by a lag owing to the alternate interlocking and release of crimped yarns.
- The presence of a textile coating can significantly reduce the crack-opening displacement. However, the presence of load oriented $T_{uncoated}$ crimped yarns resulted in the highest COD at minimum effort.
- The relationship between the maximum COD and its respective stress drop showed that the effectiveness of effort redistribution at cracking plays a crucial role in determining the crack widths.
- Finally, the modification term proposed to ε_2 values of ACK approximated the experimental values within 9.7–15%.

Further studies are required to understand the overall stress–strain and cracking behaviours of crimped textile-based TRMs formed with different types of coatings, textiles, and crimp geometries. Similarly, more supportive data are required to understand the relationship between crack width and the corresponding stress redistribution during cracking in TRMs.

Declaration of Competing Interest

The authors declare that they have no known competing financial interests or personal relationships that could have appeared to influence the work reported in this paper.

Data availability

Data will be made available on request.

References

[1] V. Mechtcherine, Novel cement-based composites for the strengthening and repair of concrete structures, Constr. Build. Mater. 41 (2013) 365–373, https://doi.org/10.1016/j.conbuildmat.2012.11.117.
[2] S.M. Raoof, L.N. Koutas, D.A. Bournas, Textile-reinforced mortar (TRM) versus fibre-reinforced polymers (FRP) in flexural strengthening of RC beams, Constr. Build. Mater. 151 (2017) 279–291, https://doi.org/10.1016/J.CONBUILDMAT.2017.05.023.
[3] L.N. Koutas, Z. Tetta, D.A. Bournas, T.C. Triantafillou, Strengthening of Concrete Structures with Textile Reinforced Mortars: State-of-the-Art Review, J. Compos. Constr. 23 (2019), https://doi.org/10.1061/(asce)cc.1943-5614.0000882.
[4] R. Nivetha, A. Vennila, B. Dharshini, A review on various properties of textile reinforced concrete, Mater. Today (2023), https://doi.org/10.1016/j.matpr.2023.05.430.
[5] A. Si Larbi, R. Contamine, P. Hamelin, TRC and hybrid solutions for repairing and/or strengthening reinforced concrete beams, 2012. ⟨https://doi.org/10.1016/j.engstruct.2012.06.002⟩.
[6] O.A. Cevallos, R.S. Olivito, Effects of fabric parameters on the tensile behaviour of sustainable cementitious composites, (2014). ⟨https://doi.org/10.1016/j.compositesb.2014.10.004⟩.
[7] M. Saidi, A. Gabor, Experimental analysis of the tensile behaviour of textile reinforced cementitious matrix composites using distributed fibre optic sensing (DFOS) technology, 2019. ⟨https://doi.org/10.1016/j.conbuildmat.2019.117027⟩.
[8] D.A. Rambo, F. De Andrade Silva, R.D. Toledo Filho, N. Ukrainczyk, E. Koenders, Tensile strength of a calcium-aluminate cementitious composite reinforced with basalt textile in a high-temperature environment, Cem. Concr. Compos 70 (2016) 183–193, https://doi.org/10.1016/j.cemconcomp.2016.04.006.
[9] T. D'Antino, C. (Corina Papanicolaou, Comparison between different tensile test set-ups for the mechanical characterization of inorganic-matrix composites, Constr. Build. Mater. 171 (2018) 140–151, https://doi.org/10.1016/J.CONBUILDMAT.2018.03.041.
[10] L. Mercedes, G. Castellazzi, E. Bernat-Maso, L. Gil, Matrix and fabric contribution on the tensile behaviour of fabric reinforced cementitious matrix composites, Constr. Build. Mater. 363 (2023) 129693, https://doi.org/10.1016/j.conbuildmat.2022.129693.
[11] V.D. Truong, D.J. Kim, A review paper on direct tensile behavior and test methods of textile reinforced cementitious composites, Compos Struct. 263 (2021), https://doi.org/10.1016/j.compstruct.2021.113661.
[12] V. Mechtcherine, K. Schneider, W. Brameshuber, Mineral-based matrices for textile-reinforced concrete, Text. Fibre Compos. Civ. Eng. (2016) 25–43, https://doi.org/10.1016/B978-1-78242-446-8.00003-3.
[13] T. Tlaiji, X.H. Vu, M. Michel, E. Ferrier, A.S. Larbi, Physical, chemical and thermomechanical characterisation of glass textile-reinforced concretes (TRC): Effect of elevated temperature and of cementitious matrix nature on properties of TRC, Mater. Today Commun. 25 (2020) 101580, https://doi.org/10.1016/j.mtcomm.2020.101580.
[14] P. Larrinaga, C. Chastre, H.C. Biscaia, J.T. San-José, Experimental and numerical modeling of basalt textile reinforced mortar behavior under uniaxial tensile stress, 2013. ⟨https://doi.org/10.1016/j.matdes.2013.09.050⟩.

[15] C. Caggegi, E. Lanoye, K. Djama, A. Bassil, A. Gabor, Tensile behaviour of a basalt TRM strengthening system: Influence of mortar and reinforcing textile ratios, 2017. ⟨https://doi.org/10.1016/j.compositesb.2017.07.027⟩.
[16] R. Contamine, A.S. Larbi, P. Hamelin, Contribution to direct tensile testing of textile reinforced concrete (TRC) composites, Mater. Sci. Eng. A 528 (2011) 8589–8598, https://doi.org/10.1016/j.msea.2011.08.009.
[17] A. Shamseldein, F. ELgabbas, H. Elshafie, Tensile behavior of basalt textile-reinforced mortar (BTRM), Ain Shams Eng. J. 13 (2022) 101488, https://doi.org/10.1016/J.ASEJ.2021.05.003.
[18] A.S.D. Rambo, F. de Andrade Silva, R.Dias Toledo Filho, O. da Fonseca Martins Gomes, Effect of elevated temperatures on the mechanical behavior of basalt textile reinforced refractory concrete, Mater. Des. (2015), https://doi.org/10.1016/j.matdes.2014.08.060.
[19] F. Zhou, H. Liu, Y. Du, L. Liu, D. Zhu, W. Pan, Uniaxial Tensile Behavior of Carbon Textile Reinforced Mortar, 12 (2019) 374, Materials Vol. 12 (2019) 374, https://doi.org/10.3390/MA12030374.
[20] A.E. Alexander, A.P. Shashikala, Experimental Investigations on the Uniaxial Tensile Behaviour of Carbon Textile Reinforced Geopolymer Mortar, Lect. Notes Civ. Eng. 269 (2023) 277–289, https://doi.org/10.1007/978-981-19-3371-4_25/COVER.
[21] J. D'Anna, G. Amato, J.F. Chen, G. Minafò, L. La Mendola, Experimental application of digital image correlation for the tensile characterization of basalt FRCM composites, Constr. Build. Mater. 271 (2021) 121770, https://doi.org/10.1016/J.CONBUILDMAT.2020.121770.
[22] A. Younis, U. Ebead, K. Shrestha, Tensile characterization of multi-ply fabric-reinforced cementitious matrix strengthening systems, Struct. Concr. 21 (2020) 713–723, https://doi.org/10.1002/SUCO.201900076.
[23] A. Peled, B. Mobasher, Z. Cohen, Mechanical properties of hybrid fabrics in pultruded cement composites, Cem. Concr. Compos 31 (2009) 647–657, https://doi.org/10.1016/J.CEMCONCOMP.2009.06.002.
[24] T. D'Antino, C. Papanicolaou, Mechanical characterization of textile reinforced inorganic-matrix composites, Compos. B (2017) 78–91, https://doi.org/10.1016/j.compositesb.2017.02.034.
[25] C. Signorini, A. Sola, A. Nobili, Hierarchical composite coating for enhancing the tensile behaviour of textile-reinforced mortar (TRM), Cem. Concr. Compos 140 (2023) 105082, https://doi.org/10.1016/J.CEMCONCOMP.2023.105082.
[26] R.-M. María, V.-L. Paula, F.-G. Jaime, L. Jorge, Improvement of tensile properties of carbon fibre-reinforced cementitious matrix composites with coated textile and enhanced mortars, Constr. Build. Mater. 369 (2023) 130552, https://doi.org/10.1016/J.CONBUILDMAT.2023.130552.
[27] A. Peled, B. Mobasher, A. Bentur, Textile Reinforced Concrete, CRC Press,, 2017, https://doi.org/10.1201/9781315119151.
[28] O. Homoro, M. Michel, T.N. Baranger, Dry mineral pre-impregnation for enhancing the properties of glass FRCM composites, 2020. ⟨https://doi.org/10.1016/j.conbuildmat.2020.120597⟩.
[29] R. Nadiv, A. Peled, V. Mechtcherine, S. Hempel, C. Schroefl, Micro- and nanoparticle mineral coating for enhanced properties of carbon multifilament yarn cement-based composites, Compos B Eng. 111 (2017) 179–189, https://doi.org/10.1016/J.COMPOSITESB.2016.12.005.
[30] J. Hegger, N. Will, O. Bruckermann, S. Voss, Load-bearing behaviour and simulation of textile reinforced concrete, Mater. Struct. 39 (2006) 765–776, https://doi.org/10.1617/s11527-005-9039-y.
[31] B. Mobasher, N. Jain, C.-M. Aldea, C. Soranakom, Mechanical Properties of Alkali Resistant Glass Fabric Composites for Retrofitting Unreinforced Masonry Walls, 2007. ⟨https://doi.org/10.14359/18756⟩.
[32] P. Valeri, M. Fernàndez Ruiz, A. Muttoni, Tensile response of textile reinforced concrete, 2020. ⟨https://doi.org/10.1016/j.conbuildmat.2020.119517⟩.
[33] A. Peled, A. Bentur, Fabric structure and its reinforcing efficiency in textile reinforced cement composites, Compos.: Part A (2003) 107–118, https://doi.org/10.1016/S1359-835X(03)00003-4.
[34] P. Preinstorfer, S. Yanik, J. Kirnbauer, J.M. Lees, A. Robisson, Cracking behaviour of textile-reinforced concrete with varying concrete cover and textile surface finish, 2023. ⟨https://doi.org/10.1016/j.compstruct.2023.116859⟩.
[35] M. Lee, M.-F. Jaime, W. Kaufmann, Load-deformation behaviour of weft-knitted textile reinforced concrete in uniaxial tension, Mater. Struct. 54 (2021), https://doi.org/10.1617/s11527-021-01797-5.
[36] E. Standard, Methods of testing cement-Part 1: Determination of strength, Turkish Standards Institute, Ankara, Turkey, 2009.
[37] W. Brameshuber, Manufacturing methods for textile-reinforced concrete, in: T. Triantafillou (Ed.), Textile Fibre Composites in Civil Engineering, 3, Woodhead Publishing, 2016, pp. 45–59, https://doi.org/10.1016/B978-1-78242-446-8.00004-5.
[38] R.T.C. 232-T. (Wolfgang Brameshuber), Recommendation of RILEM TC 232-TDT: test methods and design of textile reinforced concrete, Mater. Struct. 49 (2016) 4923–4927, https://doi.org/10.1617/s11527-016-0839-z.
[39] D. Ehlig, F. Jesse, M. Curbach, HIGH TEMPERATURE TESTS ON TEXTILE REINFORCED CONCRETE (TRC) STRAIN SPECIMENS, 2010.
[40] M. Leone, M.A. Aiello, A. Balsamo, F.G. Carozzi, F. Ceroni, M. Corradi, M. Gams, E. Garbin, N. Gattesco, P. Krajewski, C. Mazzotti, D. Oliveira, C. Papanicolaou, G. Ranocchiai, F. Roscini, D. Saenger, Glass fabric reinforced cementitious matrix: Tensile properties and bond performance on masonry substrate, Compos B Eng. 127 (2017) 196–214, https://doi.org/10.1016/J.COMPOSITESB.2017.06.028.
[41] X. Zhang, W. He, Y. Zhang, C. Chen, X. Wu, Tensile Behavior of Basalt-Fiber-Grid-Reinforced Mortar before and after Exposure to Elevated Temperature, Buildings 12 (2022), https://doi.org/10.3390/buildings12122269.
[42] R. Barhum, V. Mechtcherine, Effect of short, dispersed glass and carbon fibres on the behaviour of textile-reinforced concrete under tensile loading, Eng. Fract. Machanics (2012) 56–71, https://doi.org/10.1016/j.engfracmech.2012.06.001.
[43] G. Mattarollo, N. Randl, M. Pauletta, Investigation of the Failure Modes of Textile-Reinforced Concrete and Fiber/Textile-Reinforced Concrete under Uniaxial Tensile Tests, 16 (2023) 1999, Materials Vol. 16 (2023) 1999, https://doi.org/10.3390/MA16051999.
[44] I. Amidror, Scattered data interpolation methods for electronic imaging systems: a survey, J. Electron Imaging 11 (2002) 157–176, https://doi.org/10.1117/1.1455013.
[45] B. Mobasher, A. Peled, J. Pahilajani, Distributed cracking and stiffness degradation in fabric-cement composites, 39, Mater. Struct. 2006 39 (3) (2006) 317–331, https://doi.org/10.1007/S11527-005-9005-8.
[46] J. Aveston, G.A. Cooper, Kelly A., Single and multiple fracture. The properties of fiber composites, in: Proceedings of the Conference National Physical Laboratories., IPC Science and Technology Press, London, 1971.
[47] J. Aveston, A. Kelly, Theory of multiple fracture of fibrous composites, J. Mater. Sci. 8 (1973) 352–362, https://doi.org/10.1007/BF00550155/METRICS.
[48] P. Kapsalis, T. Triantafillou, E. Korda, D. Van Hemelrijck, T. Tysmans, Tensile Performance of Textile-Reinforced Concrete after Fire Exposure: Experimental Investigation and Analytical Approach, J. Compos. Constr. 26 (2022) 04021067, https://doi.org/10.1061/(ASCE)CC.1943-5614.0001162.